Broadband Quantum Noise Reduction in Future Long Baseline Gravitational-wave Detectors via EPR Entanglement

and

The Quantum Limits of Beam Displacement Measurements

Author
Jacob L. Beckey

Supervisors
Dr. Haixing Miao & Dr. Vincent Boyer

UNIVERSITY OF
BIRMINGHAM

June 12, 2020

Abstract

Project 1: Broadband Quantum Noise Reduction in Future Long Baseline Gravitational-wave Detectors via EPR Entanglement

Broadband quantum noise reduction can be achieved in gravitational wave detectors by injecting frequency dependent squeezed light into the the dark port of the interferometer. This frequency dependent squeezed light can be generated using external filter cavities, however in long baseline interferometers (LBIs), the filter cavity required to achieve the broadband squeezing has a low bandwidth – necessitating a very long cavity. It has been shown recently that by injecting EPR entangled beams generated in an optical parametric amplifier (OPA), the interferometer can simultaneously act as a detector and a filter cavity. This is an attractive broadband squeezing scheme for LBIs because the length requirement for the filter cavity is naturally satisfied by the length of the interferometer arms. In this project we present a systematic way of finding the working points for this broadband squeezing scheme in LBIs. We also show that in LBIs, the EPR scheme achieves nearly perfect ellipse rotation as compared to 4km interferometers which have appreciable error around the intermediate frequency. Finally, we show that an approximation for the opto-mechanical coupling constant in the 4km case breaks down for longer baselines. These results are applicable to planned detectors such as the 10km Einstein Telescope and the 40km Cosmic Explorer.

Note: A condensed version of project one has been published in Physical Review D [1]. The abstract used here is identical to the one submitted to PRD. I certify that every word written herein is my own, while acknowledging that Haixing Miao offered crucial input to the PRD draft which I, in turn, used to update the final draft of this thesis.

Abstract

Project 2: The Quantum Limits of Beam Displacement Measurements

Accurately measuring the position of a laser beam is of interest for many sensing applications including atomic force microscopy (AFM) readout. In this project, we rigorously analyze the performance of different detectors designed to measure small displacements of laser beams. We consider the performance of a linear interferometer, a single split detector, and a position sensitive detector (PSD) for coherent, as well as squeezed states of light. To the best of our knowledge, this is the first time a position sensitive detector has been treated in a rigorous quantum mechanical fashion. Our key result is the fact that a PSD should outperform a split detector when using a TEM00 beam. The methods used here are general and can be extended to other detector set-ups assuming a physical model of the detector is known.

Acknowledgements

First and foremost, I want to thank Haixing Miao and Vincent Boyer for taking me on as a student, allowing me to pursue topics that interested me, and for teaching me so much along the way. Additionally, I am thankful for the many conversations with Ellie Fradgley and Plamen Petrov which were extremely helpful in the writing of this thesis. I want to extend my gratitude to Haixing Miao and Andreas Freise for helping me return to Birmingham, and to Kai Bongs who agreed to let me do a rather uncharacteristic MRes. I am also indebted to the US-UK Fulbright Commission and the University of Birmingham for funding me.

Contents

Chapter 1

Project 1: Broadband Quantum Noise Reduction in Future Long Baseline Gravitational-wave Detectors via EPR Entanglement

1.1 Introduction and Motivation

Gravitational-wave (GW) detectors including LIGO and VIRGO, which recently made breakthrough discoveries, are Michelson-type interferometers with km size arms [2–4]. They are among the largest and most sensitive instruments humans have ever constructed. However, to push the limits of scientific discovery even further, larger, more sensitive experiments are already being planned. Two such detectors are the 10km Einstein Telescope (ET) [5] and the 40km Cosmic Explorer [6, 7]. They differ from LIGO in many ways including scale and configuration, but for our purposes can be treated in a very similar way mathematically.

All ground-based GW detectors are plagued by various noise sources that result from the fact that they are on Earth (e.g. seismic activity). Once these and all other classical noise sources are suppressed, the sensitivity of GW detectors is ultimately limited by the quantum nature of light. The quantized electromagnetic field is analogous to a quantum harmonic oscillator (position and momentum of a mass are replaced by amplitude and phase quadrature of light). The uncertainty in the amplitude and phase quadrtaures (quantum fluctuations) limits the sensitivity of interferometric measurements. One may assume that because an interferometer measures phase, we must always want lower phase noise; thus, a phase-squeezed vacuum injection would be preferable. This would be true if radiation pressure was non-existent. Because amplitude and phase are conjugate variables (like position and momentum) the Heisenberg Uncertainty Principle states that the product of their uncertainties must be greater than some constant. Thus, by decreasing phase fluc-

tuations, we suffer an increase in amplitude fluctuations. This would not be a problem if at low gravitational wave frequencies, the mirror suspension systems did not have mechanical resonances that amplify these fluctuations and make radiation pressure noise the limiting noise source [8]. Put simply, at low frequencies we need amplitude-squeezed vacuum injection. Once far away from these resonances (at higher frequencies), the detector is then limited by shot noise and thus phase-squeezed vacuum is needed. It has been known for some time that frequency-dependent squeezing would allow one to surpass the SQL over all frequencies [9]. These proposals require additional low loss filter cavities. It was shown recently; however, that this frequency-dependent squeezing can be achieved, without additional cavities, using EPR-entangled signal and idler beams (different frequency components in conventional squeezed light source) [10]. In this project, we present a systematic way of finding the working points for this broadband squeezing scheme in LBIs. We also show that in LBIs, the Einstein-Podolsky-Rosen (EPR) scheme achieves nearly perfect ellipse rotation as compared to 4km interferometers which have appreciable error. Finally, we show that an approximation for the opto-mechanical coupling constant in the 4km case can break down for longer baselines. First, though, we develop crucial quantum optics theory that will be relevant throughout this entire thesis.

1.2 Background

In order to understand the mathematics that forms the core of this project, we must first understand some content from a typical course in quantum optics. For more detail, please consult one of the standard textbooks on the subject [11–13]. If a derivation is rather specialized, I will include it in the appendix.

1.2.1 State Representation in Optical Phase Space

Quantum optics really starts with the quantization of the electromagnetic field. Refer to any textbook on quantum optics for the standard quantization of the electromagnetic field. As with the quantization of any linear theory, quantization is as simple as adding hats to the dynamical variables to make them operators in a Hilbert space. At first, this may sound like a meaningless string of words; however, as one goes through the quantization many times, it becomes clear how similar the form of the equations for the quantized field is to the classical counterpart. Decades after the first quantization of the EM field by Dirac [14], the topic is still of interest. I refer the reader to a very nice article published in 2014 on the quantization of the EM field from a physical, rather than purely mathematical point of view [15].

Once the field is quantized, we have to choose a basis in which to represent our states. A common choice is the number, or Fock, basis. In this basis, the basis vectors are of the form $|n\rangle$ where n is an integer. Thus, $|0\rangle$ represents the ground, or vacuum, state of the field. This can be thought of as the lowest energy oscillation in the field. For our purposes, we really only need to discuss the vacuum and squeezed vacuum states, because our focus is on the state that enters the unused port of the interferometer. As such, we mention here some key aspects of these states and their representation in optical phase space.

There is a one-to-one mapping between every density operator on a Hilbert space,

which we will denote ρ, and a mathematical function in optical phase called the Wigner function (named after the Hungarian-American theoretical physicist Eugene Wigner). The Wigner function is a *quasi-probability distribution*. Generally, distributions of this kind relax some of the axioms of probability theory. The Wigner function falls into this class of objects because it can take on negative values (unlike true probability distributions) and because it does not form a true joint distribution – we cannot jointly measure the two input variables because they are conjugate variables in quantum mechanics). If the state is pure (that is, if $\mathrm{tr}(\rho^2) = 1$) then the density matrix has the form $\rho = |\psi\rangle\langle\psi|$ and the Wigner function is given as:

$$W(X,Y) \equiv \int_{\infty}^{\infty} dX' \, \langle X + X'|\psi\rangle \langle\psi|X - X'\rangle \, e^{-2iX'Y} \tag{1.1}$$

Where generally, X and Y are any two conjugate observables. In our context, $\hat{X}$ will represent the amplitude quadrature of the quantized electromagnetic field and $\hat{Y}$ the phase quadrature (the hats are commonly dropped when it is clear from context what the letters represent). The quadratures are given as

$$\hat{X} = \frac{\hat{a} + \hat{a}^\dagger}{\sqrt{2}} \tag{1.2}$$

$$\hat{Y} = \frac{\hat{a} - \hat{a}^\dagger}{i\sqrt{2}} \tag{1.3}$$

where we have absorbed some factors into the definition of the creation and annihilation operators to simplify our calculations. These are directly analogous to the position and momentum operators of the quantum harmonic oscillator, respectively. The unfamiliar reader should at this time refer to one of the aforementioned standard quantum optics texts for more information.

Note that the mapping is easily generalizable to mixed states which are of the form $\rho = \sum_i p_i |\psi_i\rangle\langle\psi_i|$ (with $p_i \geq 0$ and $\sum_i p_i = 1$). In this case, the Wigner function becomes

$$W(X,Y) = \sum_i p_i W_i(X,Y) \tag{1.4}$$

where each $W_i(X,Y)$ is due to the state $|\psi_i\rangle\langle\psi_i|$ alone and is calculated using Eq. (1.1). Let us consider an important example: the Wigner function for the vacuum state $\rho = |0\rangle\langle 0|$. Recall from basic quantum mechanics that

$$\langle X + X'|0\rangle = \left(\frac{1}{\pi}\right)^{1/4} e^{-\frac{(X+X')^2}{2}} \quad \text{and} \quad \langle 0|X - X'\rangle = \left(\frac{1}{\pi}\right)^{1/4} e^{-\frac{(X-X')^2}{2}} \tag{1.5}$$

From these, we can derive the Wigner function for the vacuum state, $W_0(X,Y)$

$$W_0(X,Y) = \frac{1}{\pi} e^{-X^2 - Y^2} \tag{1.6}$$

This represents a two-dimensional distribution shown in Fig. 1.1. We typically take a cross-section of the Wigner function to visualize the state in a 2D phase space.

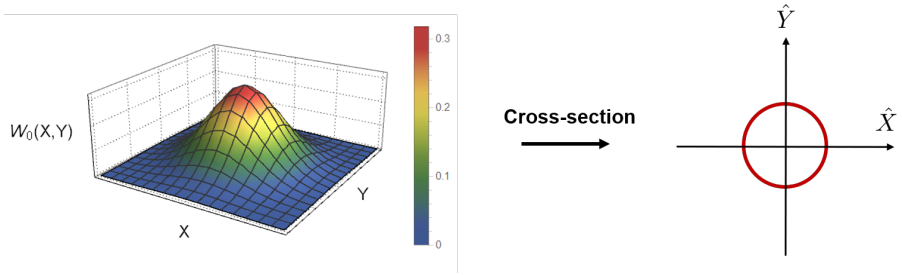

Figure 1.1: This figure shows the origin of the optical phase space representation for states. The rightmost plot shows an equiprobability contour of $W_0(X, Y)$.

We now turn to the second state we will be considering: the squeezed vacuum state. The Wigner function for the squeezed vacuum state is derived by conjugating the single-mode squeezing operator around the amplitude ($\hat{X}$) and phase ($\hat{Y}$) operators, respectively. The single-mode squeezing operator is defined as [11] as

$$S(\xi) = e^{\frac{1}{2}(\xi^* \hat{a}^2 - \xi(\hat{a}^\dagger)^2)} \quad \text{where} \quad \xi = re^{2i\theta} \tag{1.7}$$

We call θ the squeezing angle and r is the squeezing parameter. It can be shown (see aforementioned standard quantum optics text) that

$$\hat{S}^\dagger \hat{a} \hat{S} = \hat{a} \cosh r - e^{2i\theta} \hat{a}^\dagger \sinh r \tag{1.8}$$

Thus, if we focus on amplitude squeezing ($\theta = 0$) we see from the definition of the amplitude quadrature and Eq. (1.7) that

$$\hat{S}^\dagger \hat{X} \hat{S} = \frac{1}{\sqrt{2}} \left(\hat{S}^\dagger \hat{a} \hat{S} + \hat{S}^\dagger \hat{a}^\dagger \hat{S} \right) \tag{1.9}$$

$$= \frac{1}{\sqrt{2}} \left(\hat{a} \cosh r - \hat{a}^\dagger \sinh r + \hat{a}^\dagger \cosh r - \hat{a} \sinh r \right) \tag{1.10}$$

$$= \hat{X}(\cosh r - \sinh r) \tag{1.11}$$

$$\hat{S}^\dagger \hat{X} \hat{S} = e^{-r} \hat{X} \tag{1.12}$$

One can repeat the same calculation using the definition of the phase quadrature. The result is:

$$\hat{X} \to e^{-r} \hat{X} \tag{1.13}$$

$$\hat{Y} \to e^{r} \hat{Y} \tag{1.14}$$

For a phase squeezed state ($\theta = \pi/2$), the signs on the above exponentials would just flip. This yields a Wigner function of

$$W(X, Y) = \frac{1}{\pi} e^{-(e^{-r}X)^2 - (e^r Y)^2} \tag{1.15}$$

The takeaway is that the single-mode squeezing operator serves to squish our Wigner function in one direction specified by a so-called *squeezing angle*. As such, the equiprobability contour is transformed from a circle to an ellipse.

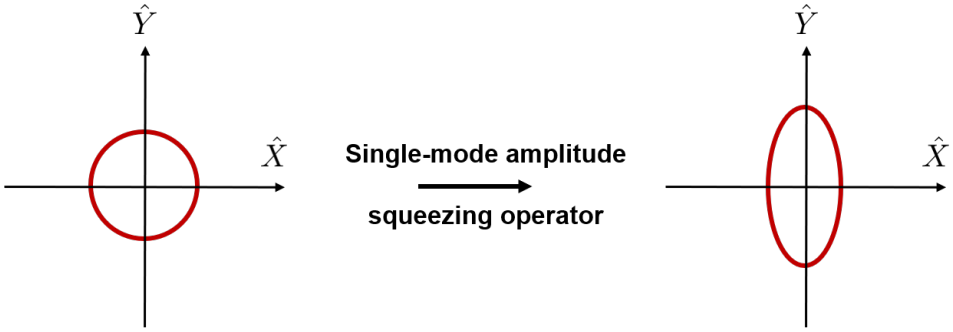

Figure 1.2: Visual representation of the action of the single-mode amplitude squeezing operator.

In order to appreciate the theory implemented in the first project, it is crucial to understand ellipse rotation. When we say ellipse rotation, we are referring to the time evolution of the equiprobability contour of the Wigner function of the squeezed vacuum state in optical phase space. We can see this rotation by solving for the time evolution of the amplitude and phase quadratures, and then calculating the time evolution of the uncertainties in these quadratures (Note: this example is adopted from Haixing Miao's course on quantum optics at University of Birmingham in Spring Term 2019).

The evolution is governed by the free Hamiltonian

$$\hat{H} = \hbar\omega(\hat{a}^\dagger\hat{a} + \frac{1}{2}) \tag{1.16}$$

There are multiple ways to derive this, but we take the following approach. We first solve the Heisenberg equation of motion for the creation and annihilation operators.

$$\dot{\hat{a}}(t) = \frac{1}{i\hbar}[\hat{a}(t), \hat{H}] \tag{1.17}$$

$$= -i\omega[\hat{a}(t), \hat{a}^\dagger(t)]\hat{a}(t) \tag{1.18}$$

$$\dot{\hat{a}}(t) = -i\omega\hat{a}(t) \tag{1.19}$$

From this we get

$$\hat{a}(t) = \hat{a}(0)e^{-i\omega t} \tag{1.20}$$

$$\hat{a}^\dagger(t) = \hat{a}^\dagger(0)e^{i\omega t} \tag{1.21}$$

Plugging back into the definition of the quadratures, we get

$$\hat{X}(t) = \frac{1}{\sqrt{2}}(\hat{a} + \hat{a}^\dagger) \tag{1.22}$$

$$= \frac{1}{2}((\hat{X}(0) + i\hat{Y}(0))e^{-i\omega t} + (\hat{X}(0) - i\hat{Y}(0))e^{i\omega t}) \tag{1.23}$$

$$= \frac{1}{2}(\hat{X}(0)(e^{-i\omega t} + e^{i\omega t}) + i\hat{Y}(0)(e^{-i\omega t} - e^{i\omega t})) \tag{1.24}$$

$$\hat{X}(t) = \hat{X}(0)\cos\omega t + \hat{Y}(0)\sin\omega t \tag{1.25}$$

Following the same procedure for the phase quadrature yields

$$\hat{Y}(t) = \hat{Y}(0)\cos\omega t - \hat{X}(0)\sin\omega t \tag{1.26}$$

Before proceeding, we must introduce the definition of the variance of a quantum operator. The variance of an operator $\hat{A}$ is defined as

$$V_{\hat{A}\hat{A}} = \langle\psi|\hat{A}^2|\psi\rangle - \langle\psi|\hat{A}|\psi\rangle^2 \tag{1.27}$$

We further define the covariance of $\hat{A}$ and $\hat{B}$ as

$$V_{\hat{A}\hat{B}} = \frac{1}{2}\langle\psi|\,\hat{A}\hat{B} + \hat{B}\hat{A}\,|\psi\rangle \tag{1.28}$$

Now, we apply these formulas to the amplitude and phase quadratures to see what we mean when we say ellipse rotation. Consider an initial state that is amplitude squeezed. In the case of the squeezed vacuum,

$$V_{\hat{X}\hat{X}} = \langle\psi|\,\hat{X}^2\,|\psi\rangle \tag{1.29}$$

$$V_{\hat{Y}\hat{Y}} = \langle\psi|\,\hat{Y}^2\,|\psi\rangle \tag{1.30}$$

$$V_{\hat{X}\hat{Y}} = \frac{1}{2}\langle\psi|\,\hat{X}\hat{Y} + \hat{Y}\hat{X}\,|\psi\rangle \tag{1.31}$$

This is true because $\langle\psi|\,\hat{X}\,|\psi\rangle = \langle\psi|\,\hat{Y}\,|\psi\rangle = 0$ for a squeezed vacuum. Using these, we get $V_{\hat{X}\hat{X}} = 1/4$, $V_{\hat{Y}\hat{Y}} = 1$, and $V_{\hat{X}Y} = 0$ at $t = 0$. So, using the equations for the time-dependent quadratures, we can calculate the variances and covariance at time t.

$$V_{\hat{X}\hat{X}} = \langle\psi|\,\hat{X}^2\,|\psi\rangle \tag{1.32}$$

$$= \langle\psi|\,(\hat{X}(0)\cos\omega t + \hat{Y}(0)\sin\omega t)^2\,|\psi\rangle \tag{1.33}$$

$$= V_{\hat{X}\hat{X}}(0)\cos^2\omega t + 2V_{\hat{X}\hat{Y}}(0)\cos\omega t\sin\omega t + V_{\hat{Y}\hat{Y}}(0)\sin^2\omega t \tag{1.34}$$

$$V_{\hat{X}\hat{X}} = \frac{1}{4}\cos^2\omega t + \sin^2\omega t \tag{1.35}$$

Following the same procedure, we find

$$V_{\hat{Y}\hat{Y}} = \frac{1}{4}\sin^2\omega t + \cos^2\omega t \tag{1.36}$$

$$V_{\hat{X}\hat{Y}} = \frac{3}{4}\cos\omega t\sin\omega t \tag{1.37}$$

Now, we can check these expressions at a few points.

	$t = 0$	$t = \frac{\pi}{4\omega}$	$t = \frac{\pi}{2\omega}$	$t = \frac{3\pi}{4\omega}$
$V_{\hat{X}\hat{X}}$	1/4	5/8	1	5/8
$V_{\hat{Y}\hat{Y}}$	1	5/8	1/4	5/8
$V_{\hat{X}\hat{Y}}$	0	3/8	0	-3/8

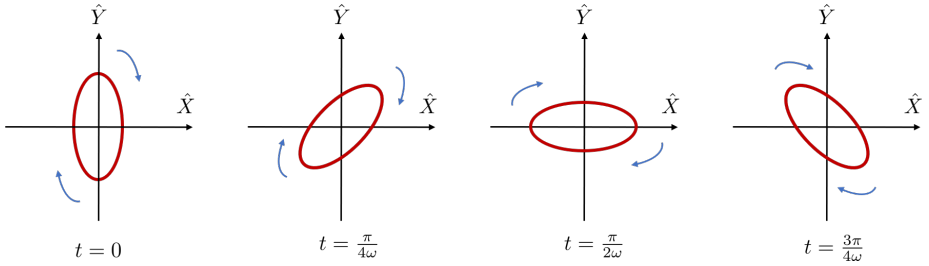

Figure 1.3: This figure, adapted from Haixing Miao's quantum optics course material, illustrates the free evolution of the squeezed state which we will call "ellipse rotation" from now on.

The takeaway is that a squeezed state will evolve freely with time. Thus, the quadrature that is squeezed will change with time. In our frequency-dependent squeezing scheme, we are essentially using the interferometer to achieve different free evolution at each individual frequency. In short, waves of different frequencies "see" a cavity with a different length. That is, they pick up a different phase depending on their frequency. This difference in free evolution allows us to use the interferometer itself as a filter cavity that yields squeezing in the desired quadrature over a range of frequencies. The relevant range of frequencies is set naturally by the length scale of the interferometer and was chosen due to the astrophysical theory at the time of inception of the detectors. More on this later. Now, we turn to the idea of a two-mode squeezed state, entanglement, and how to verify it mathematically.

1.2.2 Two-mode Squeezed State and Entanglement

Our broadband quantum noise reduction scheme takes advantage of entangled signal and idler beams generated in a nonlinear amplifier (NLA). These entangled beams can be described as a two mode squeezed state. Perhaps the simplest generation of a two mode squeezed state occurs by interfering an amplitude squeezed vacuum and a phase squeezed vacuum on a 50:50 beam splitter. As it turns out, this system serves as a great analogy to the description of the NLA. By comparing the covariance matrices for the input and output modes, we can see the signature of entanglement. For a detailed derivation of the input-output relation for the NLA in the Heisenberg picture, see Appendix A.1. We start with two fields interfering on a balanced beam splitter as shown in Fig. 1.4. It suffices to represent each field using an annihilation operator which we represent using a lowercase letter ($\hat{a}, \hat{b}$, etc.). These operators arise in the quantization of the electromagnetic field just as the raising and lowering operators for the quantum harmonic oscillator do. It is usually easier to work with just the creation and annihilation operators rather than the electric field operator but the results will be the same. Recall from introductory quantum mechanics that the creation operator "creates" a quantum of energy in our field. Another way of saying this is that the operators create a new particle in a given state. That is, they act on the number basis in the following way:

$$\hat{a} \left|n\right\rangle = \sqrt{n} \left|n-1\right\rangle \tag{1.38}$$

$$\hat{a}^\dagger \left|n\right\rangle = \sqrt{n+1} \left|n+1\right\rangle \tag{1.39}$$

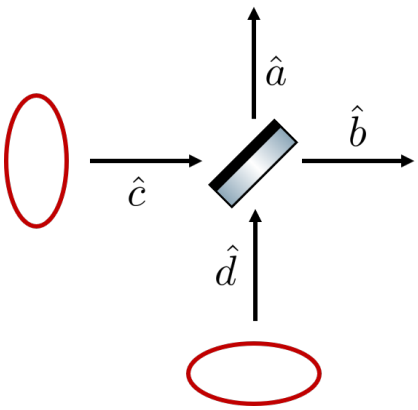

Figure 1.4: Amplitude squeezed vacuum, mode $\hat{c}$, and phase squeezed vacuum, mode $\hat{d}$, interfered on a 50:50 beam splitter.

In our case, the creation operator creates a photon in a given state and the annihilation operator removes one. The expected number of photons in a field is defined as

$$\langle \hat{N} \rangle = \langle n|\hat{a}^\dagger \hat{a}|n\rangle = n \tag{1.40}$$

Every mode of the quantized electromagnetic field is a quantum mechanical degree of freedom. We should note that classically, a mode is simply a vector field which is a normalized solution to Maxwell's equations in a vacuum [16]. The electric field operator in quantum mechanics is very similar to the classical description except that the complex field amplitudes are replaced with creation/annihilation operators. As such, our creation/annihilation operators are defined for a specific mode and the mode defines the shape in time and space of the probability of detecting a photon. For a detailed review article on the modes and states in quantum optics, see Ref. [16]. For our purposes, when you see an annihilation operator, you can think of this as one mode of a photon field. We will thus carry the manipulations out on the quantum operators themselves.

So, we start with two fields that we represent with the annihilation operators $\hat{c}$ and $\hat{d}$, where the mode corresponding to $\hat{c}$ is in an amplitude-squeezed vacuum state, and the mode corresponding to $\hat{d}$ is in a phase-squeezed vacuum state. The fields after a balanced beam splitter are given as

$$\begin{pmatrix} \hat{a} \\ \hat{b} \end{pmatrix} = \frac{1}{\sqrt{2}} \begin{pmatrix} 1 & 1 \\ 1 & -1 \end{pmatrix} \begin{pmatrix} \hat{c} \\ \hat{d} \end{pmatrix} \tag{1.41}$$

We are interested in the covariance between the amplitude and phase quadratures of these fields before and after the beam splitter. Let us define the amplitude and phase quadratures for the field represented by the annihilation operator $\hat{a}$ as

$$\hat{a}_1 = \frac{\hat{a} + \hat{a}^\dagger}{\sqrt{2}} \tag{1.42}$$

$$\hat{a}_2 = \frac{\hat{a} - \hat{a}^\dagger}{i\sqrt{2}} \tag{1.43}$$

It might make more sense to use $\hat{X}_a, \hat{Y}_a$ to represent these quadratures; however, we are adopting the notational standard set in the fundamental paper on the subject [9]. Now, the input covariance matrix is defined as

$$\mathbf{V_{in}} = \langle\psi| \begin{bmatrix} \hat{c_1} \\ \hat{c_2} \\ \hat{d}_1 \\ \hat{d}_2 \end{bmatrix} \begin{bmatrix} \hat{c_1} & \hat{c_2} & \hat{d}_1 & \hat{d}_2 \end{bmatrix} |\psi\rangle \tag{1.44}$$

$$\mathbf{V_{in}} = \langle\psi| \begin{bmatrix} \hat{c_1}\hat{c_1} & \hat{c_1}\hat{c_2} & \dots \\ \vdots & \ddots & \\ \hat{d}_2\hat{c_1} & & \hat{d}_2\hat{d}_2 \end{bmatrix} |\psi\rangle \tag{1.45}$$

An outline of how to calculate an entry of this matrix is given here, but a computer software should be used to calculate the full matrix. Calculating just one entry by hand gives a thorough appreciation of modern computers. In order to evaluate the expectation values, the form of the state needs to be known. In our set-up, the states are squeezed vacuum states which can be written as

$$|\xi\rangle = \hat{S}\,|0\rangle = e^{(\xi^*\hat{a}^2 - \xi(\hat{a}^\dagger)^2)/2}\,|0\rangle \tag{1.46}$$

where $\xi = re^{2i\theta}$ comes from the definition of the squeezing operator from Eq. (1.7) . We then use the fact that $\hat{S}^\dagger\hat{S} = \hat{I}$ and

$$\hat{S}^\dagger\hat{a}\hat{S} = \hat{a}\cosh r - e^{2i\theta}\hat{a}^\dagger \sinh r \tag{1.47}$$

where $\theta = 0$ indicates a amplitude squeezed vacuum and $\theta = \pi/2$ is phase squeezed.

$$\begin{aligned}
\langle\psi|\,\hat{c_1}\hat{c_1}\,|\psi\rangle &= \langle\psi|\,\frac{1}{\sqrt{2}}(\hat{c}+\hat{c}^\dagger)\frac{1}{\sqrt{2}}(\hat{c}+\hat{c}^\dagger)\,|\psi\rangle \\
&= \frac{1}{2}\Big(\,\langle 0|\,\hat{S}^\dagger\hat{c}\hat{c}\hat{S}\,|0\rangle + \langle 0|\,\hat{S}^\dagger\hat{c}\hat{c}^\dagger\hat{S}\,|0\rangle + \langle 0|\,\hat{S}^\dagger\hat{c}^\dagger\hat{c}\hat{S}\,|0\rangle + \langle 0|\,\hat{S}^\dagger\hat{c}^\dagger\hat{c}^\dagger\hat{S}\,|0\rangle\,\Big) \\
&= \frac{1}{2}\Big(\,\langle 0|\,\hat{S}^\dagger\hat{c}\hat{S}\hat{S}^\dagger\hat{c}\hat{S}\,|0\rangle + \langle 0|\,\hat{S}^\dagger\hat{c}\hat{S}\hat{S}^\dagger\hat{c}^\dagger\hat{S}\,|0\rangle + \dots\Big) \\
&= \frac{1}{2}\Big(\,\langle 0|\,(\hat{c}\cosh(r) - \hat{c}^\dagger e^{2i\theta}\sinh(r))(\hat{c}\cosh(r) - \hat{c}^\dagger e^{2i\theta}\sinh(r))\,|0\rangle + \dots\Big) \\
&\;\;\vdots \\
&\text{trig identities} \\
&\;\;\vdots \\
\langle\psi|\,\hat{c_1}\hat{c_1}\,|\psi\rangle &= \frac{1}{2}e^{-2r}
\end{aligned} \tag{1.48}$$

The full input covariance matrix is given as

$$\mathbf{V_{in}} = \frac{1}{2}\begin{bmatrix} e^{-2r} & 0 & 0 & 0 \\ 0 & e^{+2r} & 0 & 0 \\ 0 & 0 & e^{+2r} & 0 \\ 0 & 0 & 0 & e^{-2r} \end{bmatrix} \tag{1.49}$$

The fact that this is a diagonal matrix implies the quadratures are independent variables before interacting on the beam splitter. That is, the covariance between quadratures is zero, which is why all of the off-diagonal terms are zero. After the beam splitter, we can use the input-output relation given in Eq. (1.41) to see that covariance matrix after the beam splitter is

$$\mathbf{V_{out}} = \frac{1}{2}\begin{bmatrix} \cosh(2r) & 0 & -\sinh(2r) & 0 \\ 0 & \cosh(2r) & 0 & \sinh(2r) \\ -\sinh(2r) & 0 & \cosh(2r) & 0 \\ 0 & \sinh(2r) & 0 & \cosh(2r) \end{bmatrix} \tag{1.50}$$

I claim that this matrix indicates we have entanglement between quadratures. How can we see this? There is a simple way to mathematically verify entanglement when dealing with a bipartite state which has a Gaussian Wigner function. First, break the matrix into 2×2 blocks:

$$\mathbf{V_{out}} = \left[\begin{array}{c|c} \mathbf{V}_a & \mathbf{V}_{ab} \\ \hline \mathbf{V}_{ab} & \mathbf{V}_a \end{array}\right] \tag{1.51}$$

For example, $\mathbf{V_a}$ represents the covariance matrix for the quadratures of the field represented by the annihilation operator $\hat{a}$. By comparison with Eq. (1.50) we see that

$$\mathbf{V_a} = \langle\psi| \begin{bmatrix} \hat{a}_1 \\ \hat{a}_2 \end{bmatrix} \begin{bmatrix} \hat{a}_1 & \hat{a}_2 \end{bmatrix} |\psi\rangle = \frac{1}{2}\begin{bmatrix} \cosh(2r) & 0 \\ 0 & \cosh(2r) \end{bmatrix} \tag{1.52}$$

The determinant of a variance/covariance matrix is a generalized notion of variance. Thus, the total variance of the bipartite state outputted by the beam splitter is given by $|\mathbf{V_{out}}|$. In our case, we find

$$|\mathbf{V_{out}}| = \frac{1}{16} \tag{1.53}$$

which in our phase space normalization is a minimum uncertainty state (it saturates the relevant form of Heisenberg's uncertainty principle). However, if we calculate the same value for the input covariance matrix we also find that

$$|\mathbf{V_{in}}| = \frac{1}{16} \tag{1.54}$$

Thus, both states are minimum uncertainty states. The key is to then calculate the generalized variance of the subsystems individually. In the case of the input matrix, this is the upper-left and lower-right blocks. We have:

$$|\mathbf{V_c}| = \left| \begin{bmatrix} \frac{e^{-2r}}{2} & 0 \\ 0 & \frac{e^{2r}}{2} \end{bmatrix} \right| = \frac{1}{4} \tag{1.55}$$

$$|\mathbf{V_d}| = \left| \begin{bmatrix} \frac{e^{2r}}{2} & 0 \\ 0 & \frac{e^{-2r}}{2} \end{bmatrix} \right| = \frac{1}{4} \tag{1.56}$$

Thus, we see for the input bipartite state we have that the total uncertainty is equal to the product of the two uncertainties of the subsystems. However, for the output state, note that although $|\mathbf{V_{out}}| = \frac{1}{16}$, we have

$$|\mathbf{V_a}| = \frac{1}{4}\cosh^2(2r) \tag{1.57}$$

$$|\mathbf{V_b}| = \frac{1}{4}\cosh^2(2r) \tag{1.58}$$

Note that $\frac{1}{4}\cosh^2(2r) \geq \frac{1}{4}$ with equality if and only if $r = 0$ (no squeezing). Thus, we have a total uncertainty of $\frac{1}{16}$ but the individual systems each have uncertainty greater than $\frac{1}{4}$ (so we expect their product to be larger than 1/16). The correlation between the systems reduces the total uncertainty. This is a signature of entanglement in bipartite Gaussian quantum states. Also note that the higher the squeezing parameter, r, the larger the correlation (higher the entanglement). In the limit where $r \to \infty$, the ideal EPR case is realized. For more on this, see Ref. [17]. It is because of this entanglement that we are able to reduce the uncertainty in a given quadrature of the $\hat{a}$ field by making a measurement on a specific quadrature of the $\hat{b}$ field or vice-versa. We will now turn to the task of determining the optimal quadratures to measure in order to achieve broadband squeezing.

1.2.3 Conditional Squeezing: Reduction of Uncertainty

The concept of so-called *conditional squeezing* follows directly from the previous section. In short, we have an entangled wavefunction describing the signal and idler beams. In the limit of infinite squeezing, we have perfect quantum correlations between certain quadratures in the beams. Thus, if we measure the right quadrature in the idler beam, we will immediately collapse the wavefunction and reduce our ignorance about the signal beam due to the correlations. The higher the correlations (stronger the entanglement) the higher the noise reduction. In order to reduce the noise where we want to (i.e. conditionally) we need to determine which quadratures are correlated between the signal and idler. We can deduce this by calculating the conditional variance from first principles.

Assume the signal and idler beam are perfectly detected by a homodyne detector with strong local oscillator. Let HDa represent the signal homodyne detector which measures $\hat{a}_\theta = \hat{a}_1 \cos\theta + \hat{a}_2 \sin\theta$. Similarly for the idler, HDb measures $\hat{b}_\phi = \hat{b}_1 \cos\phi + \hat{b}_2 \sin\phi$ where $\hat{a}_1$ and $\hat{a}_2$ are the amplitude and phase quadratures defined above. Construct the following estimator of $\hat{a}_\theta$ using the measurement outcome of $\hat{b}_\phi$:

$$\hat{a}_\theta^{est} \equiv g\hat{b}_\phi \tag{1.59}$$

where $g \in [0,1]$. The conditional variance on $\hat{a}_\theta$ is defined as

$$\begin{aligned} V_{a_\theta a_\theta} &= \min_g \langle\psi| \left(\hat{a}_\theta - \hat{a}_\theta^{est}\right)^2 |\psi\rangle \\ &= \min_g \langle\psi| \left(\hat{a}_\theta - g\hat{b}_\phi\right)^2 |\psi\rangle \\ &= \min_g \langle\psi| \left(\hat{a}_\theta\hat{a}_\theta - 2g\hat{a}_\theta\hat{b}_\phi + g^2\hat{b}_\phi\hat{b}_\phi\right) |\psi\rangle \\ &= \min_g \left(V_{a_\theta a_\theta} - 2gV_{a_\theta b_\phi} + g^2 V_{b_\phi b_\phi}\right) \end{aligned} \tag{1.60}$$

Differentiating the expression in parentheses with respect to g and setting the result equal to zero, one can quickly see that the g that will minimize the conditional variance is given as

$$g_{opt} = \frac{V_{a_\theta b_\phi}}{V_{b_\phi b_\phi}} \tag{1.61}$$

We then use the definition of covariance to find the form of this optimal parameter

$$V_{\hat{A}\hat{B}} = \frac{1}{2}\langle\psi| \hat{A}\hat{B} + \hat{B}\hat{A} |\psi\rangle \tag{1.62}$$

It is then straightforward to determine that the optimal parameter is given

$$g_{opt} = \cos(\theta + \phi)\tanh 2r \tag{1.63}$$

Plugging this back into our conditional variance expression we get

$$\begin{aligned} V_{a_\theta a_\theta}|_{g=g_{opt}} &= V_{a_\theta a_\theta} - \frac{V_{a_\theta b_\phi}^2}{V_{b_\phi b_\phi}} \\ &= \frac{1}{2}\Big[\cosh(2r) - \cos^2(\theta+\phi)\sinh(2r)\tanh(2r)\Big] \end{aligned} \tag{1.64}$$

To get the minimum conditional variance, we need $\phi = -\theta$ or $\phi = \pm\pi - \theta$ (because this maximizes the term we are subtracting, thus minimizing the overall expression). As an example, let $\phi = -\pi/2$ and $\theta = \pi/2$. This yields

$$\hat{a}_1\cos(\frac{\pi}{2}) + \hat{a}_2\sin(\frac{\pi}{2}) - (\hat{b}_1\cos(-\frac{\pi}{2}) + \hat{b}_2\sin(-\frac{\pi}{2}) = \hat{a}_2 + \hat{b}_2 \tag{1.65}$$

which we call the phase sum quadrature. This quadrature will have a minimum variance. There are other combinations of quadratures that will not be at a minimum, of course. To see how conditional squeezing varies with homodyne phase (which defines what quadrature we measure) we will fix the signal phase to be $\theta = 0$ and we will vary the idler phase.

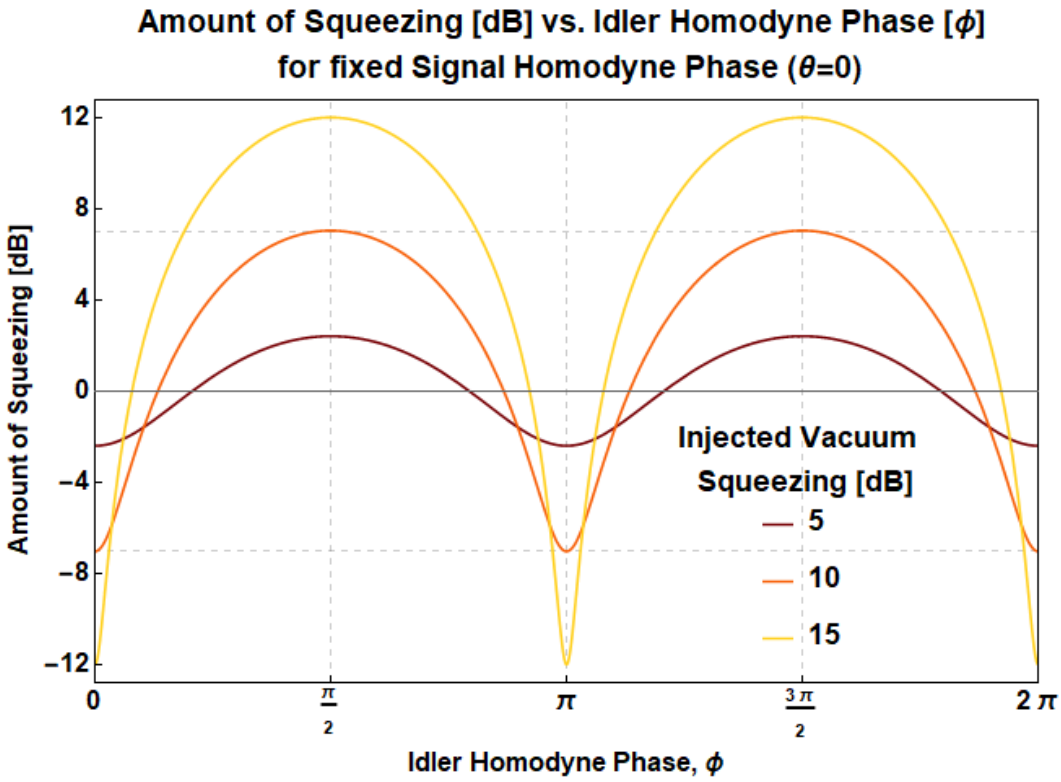

Figure 1.5: Plot showing how conditional variance or conditional squeezing changes as the quadrature combination (dictated by the signal and idler homodyne phases) changes. Note that for 15dB injected squeezing, we only retain 12dB. There is always a 3dB penalty in the EPR scheme. This is because we are measuring the idler beam to infer the quadrature of the signal beam. Thus, we will not measure as much squeezing as if we had the same total power on one beam and measured the squeezing directly [10, 18].

When the homodyne phases are chosen optimally ($\theta = -\phi$ we get the minimum conditional variance

$$\begin{aligned} V_{a_\theta a_\theta}|_{g=g_{opt}} &= \frac{1}{2}\Big[\cosh(2r) - \sinh(2r)\tanh(2r)\Big] \\ &= \frac{1}{\cosh(2r)} \end{aligned} \tag{1.66}$$

Looking at the graph of this function, we see that the conditional variance very quickly goes to zero. Thus with moderately high squeezing, measuring the idler quadrature, $\hat{b}_\theta$, allows us to accurately predict the signal quadrature $\hat{a}_{-\theta}$. By measuring the idler, then, we are reducing our ignorance and squeezing the chosen quadrature by a factor of $1/\cosh 2r$.

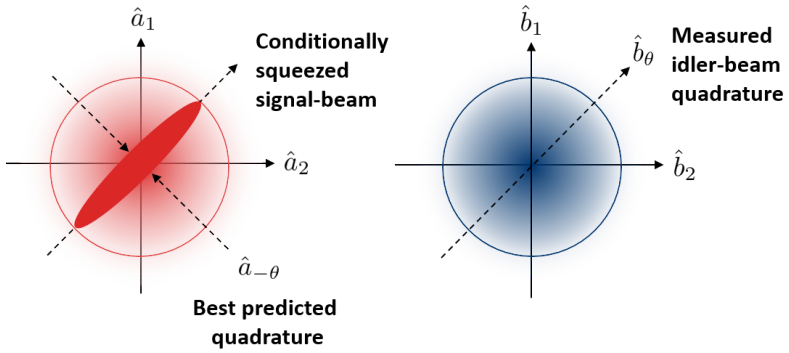

Figure 1.6: The signal and idler states represented in optical phase space. By measuring the idler quadrature $\hat{b}_\theta$ we reduce the uncertainty in the signal quadrature $\hat{a}_{-\theta}$ by $\cosh 2r$. Note this figure was directly adopted from [10].

1.2.4 EPR Entanglement in a Detuned Optical Parametric Amplifier

In general, a non-degenerate optical parametric amplifier (OPA) takes in a "seed" beam and a pump beam (energy source) and produces two correlated beams at different frequencies. We can learn a lot about this process by examining the interaction Hamiltonian for the system. This is given as [11]

$$\hat{H}_{int} = i\hbar\chi^{(2)}\alpha_p\big(a^\dagger b^\dagger - ab\big) \tag{1.67}$$

We see that the interaction depends on the strength of the pump, α_p, as well as the nonlinear susceptibility of the material $\chi^{(2)}$. Nonlinearities of this type can be found in crystals with certain symmetries (or rather, asymmetries). From this Hamiltonian, we are able to derive the input-output relation of the NLA (or more specifically, the OPA). Please see Appendix A.1 for this derivation. The crucial bit of theory is given here.

Consider a squeezer with broad squeezing spectrum ($\sim$ 100 MHz). In our EPR-based broadband squeezing scheme, the injected light is intentionally offset from the carrier frequency, ω_0 by some $\Delta/2$ where Δ is of order MHz. This generates correlated sidebands

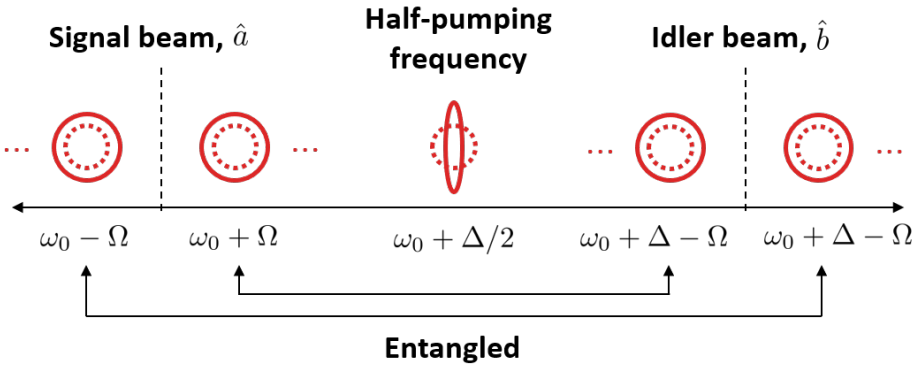

Figure 1.7: Visualization of the frequency-mode entanglement in the pumped OPA in our proposed scheme.

around ω_0 and $\omega_0 + \Delta$ as shown in Fig. 1.7. We introduce the following annihilation operators to describe our four sidebands

$$\hat{a}_\pm \equiv \hat{a}(\omega_0 \pm \Omega) \qquad \hat{b}_\pm \equiv \hat{b}(\omega_0 + \Delta \pm \Omega) \tag{1.68}$$

Where Ω is the audio-sideband frequency. A sideband at this frequency would be induced by a incident gravitational wave and will thus be relevant as we continue our discussion of squeezing. We will consider a squeezer with squeezing factor, r, and squeezing angle ϕ. Our squeezer is non-degenerate (meaning the output modes are at different frequencies). We will have a two mode squeezed state coming out of the squeezer. The transformations on our creation and annihilation operators needed to derive the output state are

$$\hat{S}^\dagger \hat{b}_\pm \hat{S} = \hat{b}_\pm \cosh r - \hat{a}_\mp^\dagger e^{2i\phi} \sinh r \tag{1.69}$$

$$\hat{S}^\dagger \hat{b}_\pm^\dagger \hat{S} = \hat{b}_\pm^\dagger \cosh r - \hat{a}_\mp e^{-2i\phi} \sinh r \tag{1.70}$$

$$\hat{S}^\dagger \hat{a}_\mp \hat{S} = \hat{a}_\mp \cosh r - \hat{b}_\pm^\dagger e^{2i\phi} \sinh r \tag{1.71}$$

$$\hat{S}^\dagger \hat{a}_\mp^\dagger \hat{S} = \hat{a}_\mp^\dagger \cosh r - \hat{b}_\pm e^{-2i\phi} \sinh r \tag{1.72}$$

where $\hat{S}$ is the squeezing operator defined previously such that $\hat{S}\,|0\rangle = |\xi\rangle$. Note that we take $\phi = \pi/2$ to be amplitude squeezed and $\phi = 0$ to be phase squeezed as is the convention of Kimble et al. [9]. Thus, we see that the squeezing operator serves to "mix" our sidebands. We said that entanglement was generated, but how can we verify this? In the single frequency-mode case, all we had to do was calculate the covariance matrix and compute some determinants. We follow a similar procedure here; however, because we are looking at the spectrum of positive frequencies, we must calculate the spectral density. The noise spectral density can just be thought of as the variance of the operator (quantum noise) at each frequency. We can then generate a noise spectral density matrix and calculate the relevant determinants needed to verify entanglement as long as the underlying states have Gaussian wigner functions (see Sec. 1.2.2). The single-sided spectral density is defined as

$$S_{\hat{A}\hat{B}}\delta(\Omega - \Omega') = \frac{1}{2\pi} \langle\psi|\, \hat{A}(\Omega)\hat{B}^\dagger(\Omega') + \hat{B}^\dagger(\Omega')\hat{A}(\Omega)\,|\psi\rangle \tag{1.73}$$

The noise spectral densities can be measured with spectral analyzers in the lab. Sometimes, two-sided spectral densities (which allow for positive and negative frequencies) are used. In this case we only positive frequencies and think of the quantity as the variance or covariance of a given operator at a given frequency. For more on the notion of single-sided noise spectral density, see Refs. [9, 19] or any resource on signal analysis. Applying this formula, we can derive the spectral density matrix (see Appendix A.2 for a detailed example) as

$$S = \begin{bmatrix} S_{\hat{a}_1\hat{a}_1} & S_{\hat{a}_1\hat{a}_2} & S_{\hat{a}_1\hat{b}_1} & S_{\hat{a}_1\hat{b}_2} \\ S_{\hat{a}_2\hat{a}_1} & S_{\hat{a}_2\hat{a}_2} & S_{\hat{a}_2\hat{b}_1} & S_{\hat{a}_2\hat{b}_2} \\ S_{\hat{b}_1\hat{a}_1} & S_{\hat{b}_1\hat{a}_2} & S_{\hat{b}_1\hat{b}_1} & S_{\hat{b}_1\hat{b}_2} \\ S_{\hat{b}_2\hat{a}_1} & S_{\hat{b}_2\hat{a}_2} & S_{\hat{b}_2\hat{b}_1} & S_{\hat{b}_2\hat{b}_2} \end{bmatrix} \tag{1.74}$$

$$S = \begin{bmatrix} \cosh 2r & 0 & \cos 2\phi \sinh 2r & \sin 2\phi \sinh 2r \\ 0 & \cosh 2r & \sin 2\phi \sinh 2r & -\cos 2\phi \sinh 2r \\ \cos 2\phi \sinh 2r & \sin 2\phi \sinh 2r & \cosh 2r & 0 \\ \sin 2\phi \sinh 2r & -\cos 2\phi \sinh 2r & 0 & \cosh 2r \end{bmatrix} \tag{1.75}$$

If we focus on amplitude squeezing ($\phi = \pi/2$) this matrix just reduces to the single mode case derived in Section 1.2.2. This tells us that the type of entanglement is essentially the same. There are other, more mathematically rigorous, entanglement criteria; however, for our purposes it is sufficient to note that a non-zero off diagonal term in a covariance or spectral density matrix indicates entanglement. At the end of the day, it is this entanglement that will allow us to reduce the noise in our GW detector.

1.3 Theory

Now that we have covered the background quantum optics needed to understand the theory in this project, we are able to get started deriving key expressions. As you will see, much of the theory below is a specific case of the expressions derived above. We adopt the notations that are standard in the GW community and leave the lengthiest calculations for the appendix.

1.3.1 Derivation of the Detector Sensitivity

We first derive the sensitivity formula for the gravitational-wave detector with the EPR squeezing scheme implemented. This section follows the supplementary materials from the original paper on this scheme [10]. However, I will carry the derivation out in much more detail, adding explanation along the way.

First, we assign creation and annihilation operators to each sideband frequency, Ω. A pumped optical parametric amplifier (OPA) is used to generate the two-mode squeezed state that enters the dark port of the interferometer. The full derivation of the input-output

relation for the non-degenerate OPA is given in the first section of Appendix A. The result for the upper sidebands is

$$\hat{a}(\omega_0 + \Omega) = \mu \hat{a}_{in}(\omega_0 + \Omega) + \nu \hat{b}^\dagger_{in}(\omega_0 + \Delta - \Omega) \tag{1.76}$$

$$\hat{b}(\omega_0 + \Delta + \Omega) = \mu \hat{b}_{in}(\omega_0 + \Delta + \Omega) + \nu \hat{a}^\dagger_{in}(\omega_0 - \Omega) \tag{1.77}$$

where the coefficients μ and ν can be written as $\mu = \cosh r$ and $\nu = \sinh r$. Here, the squeezing parameter r depends on the $\chi^{(2)}$ nonlinearity coefficient of the amplifying medium, the pump field strength, and the interaction time. To obtain the operators for the lower sidebands, just take the Hermitian conjugate of equations (1.76) and (1.77).

This method of modelling sidebands using frequency-dependent creation and annihilation operators is called "two-photon formalism" and dates back to 1985 in the work of Carlton M. Caves [20]. It has become a standard in the gravitational-wave community. In this formalism, we define the amplitude and phase quadratures of the signal and idler fields as

$$\begin{aligned} \hat{a}_1(\Omega) &= \frac{\hat{a}(\omega_0 + \Omega) + \hat{a}^\dagger(\omega_0 - \Omega)}{\sqrt{2}} \\ \hat{a}_2(\Omega) &= \frac{\hat{a}(\omega_0 + \Omega) - \hat{a}^\dagger(\omega_0 - \Omega)}{i\sqrt{2}} \end{aligned} \tag{1.78}$$

$$\begin{aligned} \hat{b}_1(\Omega) &= \frac{\hat{b}(\omega_0 + \Delta + \Omega) + \hat{b}^\dagger(\omega_0 + \Delta - \Omega)}{\sqrt{2}} \\ \hat{b}_2(\Omega) &= \frac{\hat{b}(\omega_0 + \Delta + \Omega) - \hat{b}^\dagger(\omega_0 + \Delta + \Omega)}{i\sqrt{2}} \end{aligned} \tag{1.79}$$

where $\hat{o}_1$ denotes the amplitude quadrature for mode o and $\hat{o}_2$ denotes the phase quadrature for the same mode. Having written the frequencies down explicitly this first time, we will drop them in future manipulations as it is very cumbersome.

Using homodyne detection, one can detect any quadrature of the optical field given an appropriate phase reference. If we have two homodyne detectors, one for the $\hat{a}$-field and one for the $\hat{b}$-field, we can detect any quadrature of both fields. The output of homodyne detection is really just a photocurrent, so we can experimentally add or subtract the photocurrents from the two homodyne detectors to create so-called "joint quadratures" for the $\hat{a}$ and $\hat{b}$ fields. For example, consider the amplitude sum quadrature $\hat{a}_1 + \hat{b}_1$. From

equations (1.76) and (1.77), we have

$$\begin{aligned}
\hat{a}_1 + \hat{b}_1 &= \frac{\hat{a} + \hat{a}^\dagger}{\sqrt{2}} + \frac{\hat{b} + \hat{b}^\dagger}{\sqrt{2}} \\
&= \frac{\mu\hat{a}_{in} + \nu\hat{b}_{in}^\dagger + \mu\hat{a}_{in}^\dagger + \nu\hat{b}_{in} + \mu\hat{b}_{in} + \nu\hat{a}_{in}^\dagger + \mu\hat{b}_{in}^\dagger + \nu\hat{a}_{in}}{\sqrt{2}} \\
&= \frac{(\mu+\nu)(\hat{a}_{in} + \hat{a}_{in}^\dagger)}{\sqrt{2}} + \frac{(\mu+\nu)(\hat{b}_{in} + \hat{b}_{in}^\dagger)}{\sqrt{2}} \\
&= (\cosh r + \sinh r)(\hat{a}_{1,in} + \hat{b}_{1,in}) \\
&= (\frac{e^r + e^{-r}}{2} + \frac{e^r - e^{-r}}{2})(\hat{a}_{1,in} + \hat{b}_{1,in}) \\
\hat{a}_1 + \hat{b}_1 &= e^r(\hat{a}_{1,in} + \hat{b}_{1,in})
\end{aligned} \tag{1.80}$$

The uncertainties are thus related by

$$\Delta(\hat{a}_1 + \hat{b}_1) = e^r \Delta(\hat{a}_{1,in} + \hat{b}_{1,in}) \tag{1.81}$$

In other words, the uncertainty for the amplitude sum quadrature is amplified by e^r. Following these same steps, one can derive the other joint quadratures. The result is

$$\hat{a}_1 + \hat{b}_1 = e^r(\hat{a}_{1,in} + \hat{b}_{1,in}) \qquad \hat{a}_1 - \hat{b}_1 = e^{-r}(\hat{a}_{1,in} - \hat{b}_{1,in}) \tag{1.82}$$

$$\hat{a}_2 + \hat{b}_2 = e^{-r}(\hat{a}_{2,in} + \hat{b}_{2,in}) \qquad \hat{a}_2 - \hat{b}_2 = e^r(\hat{a}_{2,in} - \hat{b}_{2,in}) \tag{1.83}$$

We can calculate the uncertainties and show that two joint quadratures are squeezed and two are anti-squeezed. Now, because the commutator between the phase sum and amplitude difference quadratures is zero, those joint quadratures may be squeezed simultaneously without violating the Heisenberg uncertainty principle. It was pointed out 30 years ago that a non-degenerate parametric amplifier could provide an experimental realization of the famous EPR paradox [17, 21]. In analogy to the original EPR argument, $\hat{b}_1$ is correlated with $\hat{a}_1$, while $\hat{b}_2$ is correlated with $-\hat{a}_2$. More generally, $\hat{b}_\theta = \hat{b}_1 \cos\theta + \hat{b}_2 \sin\theta$ is correlated with $\hat{a}_{-\theta} = \hat{a}_1 \cos\theta - \hat{a}_2 \sin\theta$.

With a homodyne detector for both the signal and idler fields, both $\hat{a}_{-\theta}$ and $\hat{b}_\theta$ can be detected. To obtain the joint quadratures, we combine the outputs of the two homodyne detectors. It turns out that simply summing or taking the difference of the quadratures is not optimal [22]. To achieve the optimal measurement, the idler field quadrature $\hat{b}_\theta$ is filtered before being combined with the signal field quadrature. The final expression for the filtered joint quadrature is given as

$$\begin{aligned}
\hat{a}_{-\theta}^g &= \hat{a}_{-\theta} - g\hat{b}_\theta \\
&= \hat{a}_1 \cos\theta - \hat{a}_2 \sin\theta - g(\hat{b}_1 \cos\theta + \hat{b}_2 \sin\theta) \\
\hat{a}_{-\theta}^g &= (\hat{a}_1 - g\hat{b}_1)\cos\theta - (\hat{a}_2 + g\hat{b}_1)\sin\theta
\end{aligned} \tag{1.84}$$

We now calculate the spectral density of this filtered joint quadrature operator.

$$\begin{aligned}
S_{\hat{a}_{-\theta}^g \hat{a}_{-\theta}^g}\delta(\Omega - \Omega') &= \frac{1}{2\pi}\langle\psi|\, \hat{a}_{-\theta}^g (\hat{a}_{-\theta}^g)^\dagger + (\hat{a}_{-\theta}^g)^\dagger \hat{a}_{-\theta}^g \,|\psi\rangle \\
&= S_{\hat{a}_{-\theta}\hat{a}_{-\theta}} - gS_{\hat{a}_{-\theta}\hat{b}_\theta} - gS_{\hat{b}_\theta\hat{a}_{-\theta}} + g^2 S_{\hat{b}_\theta\hat{b}_\theta} \\
S_{\hat{a}_{-\theta}^g \hat{a}_{-\theta}^g} &= \cosh 2r - g\cos 2\phi \sinh 2r - g\cos 2\phi \sinh 2r + g^2 \cosh 2r
\end{aligned} \tag{1.85}$$

where ϕ here is the squeezing angle from the two-mode squeezing operator. For phase squeezing injection, $\phi = 0$. So, we have

$$\begin{aligned} S_{\hat{a}^g_{-\theta}\hat{a}^g_{-\theta}} &= (1+g^2)\cosh 2r - 2g\sinh 2r \\ &= (1+g^2)(\cosh^2 r + \sinh^2 r) - 2g(2\sinh r\cosh r) \\ &= \cosh^2 r - 2g\sinh r\cosh r + g^2\sinh^2 r + g^2\cosh^2 r - 2g\sinh r\cosh r + \sinh^2 r \\ &= (\cosh r - g\sinh r)^2 + (g\cosh r - \sinh r)^2 \\ S_{\hat{a}^g_{-\theta}\hat{a}^g_{-\theta}} &= (\mu - g\nu)^2 + (\nu - g\mu)^2 \end{aligned} \tag{1.86}$$

To realize the optimal squeezing spectrum, we need to solve for the filter that minimizes the above spectrum. Thus we differentiate equation (1.86) and set the result equal to zero and then solve for g.

$$\begin{aligned} \frac{\partial S_{\hat{a}^g_{-\theta}\hat{a}^g_{-\theta}}}{\partial g} &= 0 \\ 2(\mu - g\nu)(-\nu) + 2(\nu - g\mu)(-\mu) &= 0 \\ -\mu\nu + g\nu^2 &= \mu\nu - g\mu^2 \\ g(\nu^2 + \mu^2) &= 2\mu\nu \\ g_{opt} &= \frac{2\mu\nu}{\nu^2 + \mu^2} \\ g_{opt} &= \tanh 2r \end{aligned} \tag{1.87}$$

Using the optimal filter, our spectrum becomes

$$\begin{aligned} S^{g_{opt}}_{\hat{a}^g_{-\theta}\hat{a}^g_{-\theta}} &= (1+\tanh^2 2r)\cosh 2r - 2\tanh 2r\sinh 2r \\ &= \cosh 2r + \frac{\sinh^2 2r}{\cosh 2r} - 2\frac{\sinh^2 2r}{\cosh 2r} \\ &= \frac{\cosh^2 2r - \sinh^2 2r}{\cosh 2r} \\ S^{g_{opt}}_{\hat{a}^g_{-\theta}\hat{a}^g_{-\theta}} &= \frac{1}{\cosh 2r} \end{aligned} \tag{1.88}$$

We can compare this to the single mode case in section 1.2.3 to see that the result is identical. This is because the nature of the entanglement in the single and multi-frequency-mode case is identical. Now, because this noise spectrum quickly goes to zero, the correlation between $\hat{a}_{-\theta}$ and $\hat{b}_\theta$ quickly goes to one. Thus, by measuring the idler field quadrature, one can predict the signal field quadrature with great accuracy.

In gravitational wave interferometers, the signal is detected in the phase quadrature at the dark port. Thus, to calculate the sensitivity of an interferometer, we need to know the form of the phase quadrature upon exiting the interferometer. The input-ouput relation of the quantum noise in the signal channel is given as [9]:

$$\hat{A}_2 = e^{2i\beta}(\hat{a}_2 - \mathcal{K}\hat{a}_1) \tag{1.89}$$

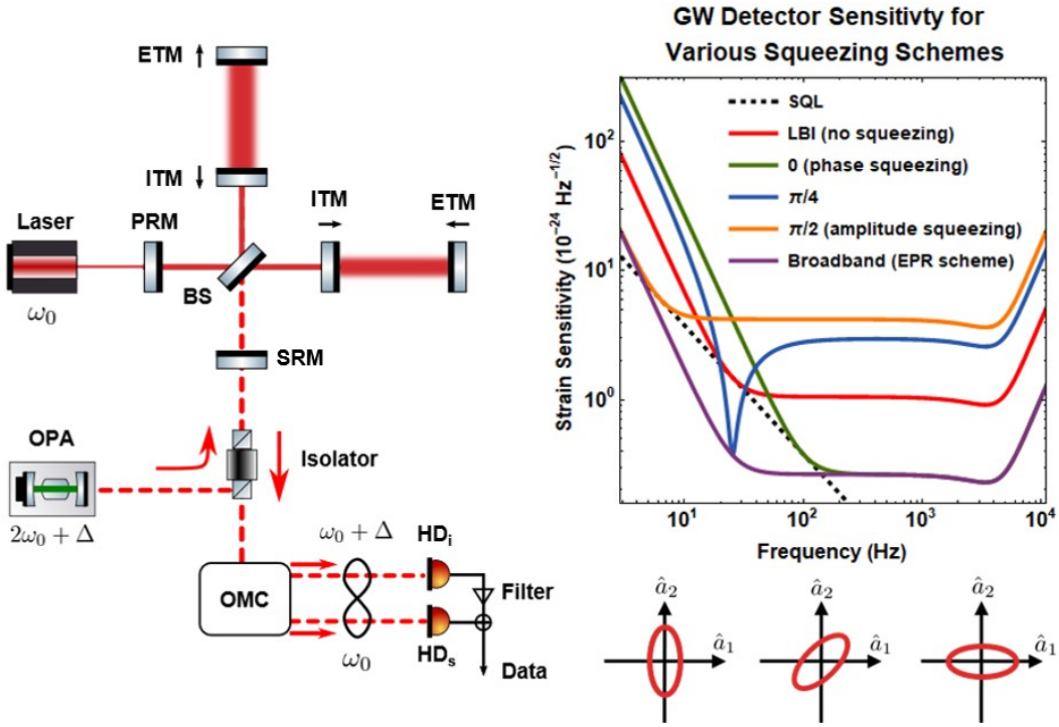

Figure 1.8: LBI setup and sensitivity curves for various squeezing schemes. A fixed squeezing angle only surpasses the SQL (black dotted line) over a narrow frequency band. Our broadband squeezing scheme (purple curve) is achieved by rotating the noise ellipse in a frequency-dependent way as shown below the plot. Acronyms used are: end test mirror (ETM), input test mirror (ITM), power recycling mirror (PRM), signal recycling mirror (SRM), and output mode cleaner (OMC).

where $\mathcal{K}$ is an opto-mechanincal coupling constant which serves to couple amplitude fluctuations to phase fluctuations and is given as

$$\mathcal{K} = \frac{2h_{\mathrm{SQL}}^2 L_{\mathrm{arm}} \omega_0 P_{\mathrm{arm}} \gamma \omega_s^2}{\hbar c[\gamma^2 \Omega^2 + (\Omega^2 - \omega_s^2)^2]} \tag{1.90}$$

where h_{SQL}^2 is the standard quantum limit for the single-sided spectral density, L_{arm} is the interferometer arm length, ω_0 the laser frequency, P_{arm} the circulating power of the interferometer arm, Ω the sideband (and GW signal) frequency, ω_s is a resonant frequency that arises from the coupling between the signal recycling and arm cavities [23]. The frequency and bandwidth for this resonance are given as

$$\omega_s = \frac{cT_{\mathrm{ITM}}}{2\sqrt{L_{\mathrm{arm}} L_{\mathrm{SRC}}}} \tag{1.91}$$

$$\gamma = \frac{cT_{\mathrm{SRM}}}{4L_{\mathrm{SRC}}} \tag{1.92}$$

Equation (1.89) can also be written as

$$\hat{A}_2 = e^{2i\beta}(\sqrt{1+\mathcal{K}^2})(\hat{a}_1 \cos\xi - \hat{a}_2 \sin\xi) \tag{1.93}$$

where $\xi = -\arctan\frac{1}{\mathcal{K}}$. As the connection between these two equations is not immediately clear, it is worth going through now. First, note that

$$\sin(\arctan x) = \frac{x}{\sqrt{1+x^2}} \qquad \cos(\arctan x) = \frac{1}{\sqrt{1+x^2}} \tag{1.94}$$

So we can write the following

$$\begin{aligned}
\hat{A}_2 &= e^{2i\beta}(\sqrt{1+\mathcal{K}^2})(\hat{a}_1\cos\xi - \hat{a}_2\sin\xi) \\
&= e^{2i\beta}(\sqrt{1+\mathcal{K}^2})(\hat{a}_1\cos(-\arctan\frac{1}{\mathcal{K}}) - \hat{a}_2\sin(-\arctan\frac{1}{\mathcal{K}})) \\
&= e^{2i\beta}(\sqrt{1+\mathcal{K}^2})(\hat{a}_1(\frac{1}{\sqrt{1+\frac{1}{\mathcal{K}^2}}}) + \hat{a}_2\frac{\frac{1}{\mathcal{K}}}{\sqrt{1+\frac{1}{\mathcal{K}^2}}}) \\
&= e^{2i\beta}(\sqrt{1+\mathcal{K}^2})(\hat{a}_1(\frac{-\mathcal{K}}{\sqrt{1+\mathcal{K}^2}}) + \hat{a}_2\frac{1}{\sqrt{1+\mathcal{K}^2}}) \\
\hat{A}_2 &= e^{2i\beta}(\hat{a}_2 - \mathcal{K}\hat{a}_1)
\end{aligned} \tag{1.95}$$

Note that the negative sign on the $\mathcal{K}$ in the second to last line is valid because we took a $1/\mathcal{K}^2$ out from under the square root, so we have the freedom to take either the positive or negative root. Thus, we see that the expressions are in fact equivalent. The reason for writing this expression in a seemingly more complex way than Eq. (1.89) is to illuminate that the quadrature of the signal field that is outputted by the interferometer is $-\arctan\frac{1}{\mathcal{K}}$. The important point is that it is a function of the opto-mechanical coupling constant $\mathcal{K}$ and thus a function of interferometer parameters. Thus, to maximize the correlation between the signal and idler field, we would want to detect the idler quadrature $\hat{b}_{\arctan\frac{1}{\mathcal{K}}}$ because $\hat{a}_{-\theta}$ is maximally correlated with $\hat{b}_\theta$. Ideally, then, we would detect

$$\hat{B}_2 = e^{i\alpha}(-\hat{b}_1\sin\Phi_{\text{rot}} + \hat{b}_2\cos\Phi_{\text{rot}}) \tag{1.96}$$

where $e^{i\alpha}$ is an unimportant phase factor accumulated as the sidebands propagate through the interferometer and $\Phi_{\text{rot}} = \arctan\mathcal{K}$. So, assuming we can design the interferometer so that our noise ellipse rotates by a total angle $\Phi_{\text{rot}} = \arctan\mathcal{K}$ throughout the length of the interferometer, we would then filter the output and combine it with the signal field as mentioned above

$$\hat{A}_2^g = \hat{A}_2 - g\hat{B}_2 \tag{1.97}$$

The rest of this derivation just becomes a special case of the general method above, so not as much detail will be shown. The spectral density for this filtered joint quadrature is given as

$$S_{\hat{A}_2^g\hat{A}_2^g} = S_{\hat{A}_2\hat{A}_2} - gS_{\hat{A}_2\hat{B}_2} - gS_{\hat{B}_2\hat{A}_2} + g^2S_{\hat{B}_2\hat{B}_2} \tag{1.98}$$

Differentiating this expression with respect to g, setting equal to zero, and solving for g yields

$$g_{\text{opt}} = \frac{S_{\hat{A}_2\hat{B}_2}}{S_{\hat{B}_2\hat{B}_2}} \tag{1.99}$$

Remembering that the injected squeezing angle is taken to be $\phi = 0$, we find

$$g_{\text{opt}} = \frac{S_{\hat{A}_2\hat{B}_2}}{S_{\hat{B}_2\hat{B}_2}} = \frac{e^{i(2\beta-\alpha)}\sqrt{1+\mathcal{K}^2}\sinh 2r}{\cosh 2r} = e^{i(2\beta-\alpha)}\sqrt{1+\mathcal{K}^2}\tanh 2r \tag{1.100}$$

Plugging equation (1.100) into equation (1.98) we see

$$S^{g_{\rm opt}}_{\hat{A}_2\hat{A}_2} = S_{\hat{A}_2\hat{A}_2} - \frac{S_{\hat{B}_2\hat{A}_2}S_{\hat{A}_2\hat{B}_2}}{S_{\hat{B}_2\hat{B}_2}} = \frac{1+\mathcal{K}^2}{\cosh 2r} \tag{1.101}$$

This equation is the conditional squeezing spectrum of the quantum noise exiting the interferometer. If there is a gravitational wave present, the signal becomes [9]:

$$\hat{A}_2^{GW} = \sqrt{2\mathcal{K}}e^{i\beta}\frac{h}{h_{\rm SQL}} \tag{1.102}$$

With this as the signal field and Eq. (1.96) as the idler field, the spectral density for the interferometer with EPR squeezing ideally implemented is given as

$$S_h = \frac{h^2_{\rm SQL}}{2\cosh 2r}\left(\mathcal{K}+\frac{1}{\mathcal{K}}\right) \tag{1.103}$$

If you compare this to Eq. (27) from Ref. [9], you will see that the EPR squeezing scheme provides a $\cosh 2r$ suppression of quantum noise.

1.3.2 Approximating Rotation Angle

We cannot achieve the ideal rotation angle without a separate filter cavity. If we are going to approximate the rotation angle, then, we need to bound the error to ensure we achieve comparable broadband noise reduction.

An expression that takes into account both the exact and approximate rotation angle is given in Eq. (46) of reference [9]:

$$S_h = \frac{h^2_{\rm SQL}}{2}\left(\frac{1}{\mathcal{K}}+\mathcal{K}\right)\left(\cosh 2R - \cos\left[2(\Phi^{\rm approx}_{\rm rot}+\Phi_{\rm rot})\right]\sinh 2R\right) \tag{1.104}$$

As this expression currently stands, we cannot apply it to our setup because the R in this expression and the r in our expressions thus far refer to two different squeezing parameters. Thus, we need to solve for R in terms of r and then substitute back into Eq. (1.103). Comparing Eq. (48) from KLMTV to Eq. (1.103) we see that

$$e^{-2R} = \frac{1}{\cosh 2r} \tag{1.105}$$

which implies

$$R = \frac{1}{2}\ln\left(\cosh 2r\right) \tag{1.106}$$

Now, plugging Eq. (1.106) into Eq. (1.103) and assuming $\delta\Phi = \Phi^{\rm approx}_{\rm rot} << 1$ so that we can use a second order Taylor series approximation for cosine, we get

$$\begin{aligned} S_h &\approx \frac{h^2_{\rm SQL}}{2}\left(\frac{1}{\mathcal{K}}+\mathcal{K}\right)\left(\frac{\cosh^2 2r+1}{2\cosh 2r} - (1-2\delta\Phi^2)\frac{\cosh^2 2r-1}{2\cosh 2r}\right) \\ S_h &\approx \frac{h^2_{\rm SQL}}{2\cosh 2r}\left(\mathcal{K}+\frac{1}{\mathcal{K}}\right) + \frac{h^2_{\rm SQL}}{2}\frac{\sinh^2 2r}{\cosh 2r}\left(\mathcal{K}+\frac{1}{\mathcal{K}}\right)\delta\Phi^2 \end{aligned} \tag{1.107}$$

where the first term is the exact value and the second term is an error term due to not realizing the rotation angle precisely. The ratio between the error term and the exact value is $\sinh^2(2r)\delta\Phi^2$. In the case of a 15dB squeezing injection as considered in [10], $r = 1.73$, so the correction term is $\approx 249\delta\Phi^2$. So, if we want to keep the relative correction to less than 10%, we will need the error in the rotation angle $\delta\Phi < 0.02$ rad.

$$249(0.02 \text{ rad})^2 \times 100\% = 9.96\% < 10\% \tag{1.108}$$

So, as long as the proposed scheme keeps the overall error in the rotation angle to less than 0.02 rad, we will suffer no more than a 10% degradation in noise reduction. This bound will heavily restrict our parameter space as we will see in the next section.

1.4 Results

In the case where we implement long, low loss external filter cavities, the ideal rotation angle would be $\Phi_{\text{rot}} = \arctan\mathcal{K}$. However, we propose to use the signal recycling interferometer itself as the filter cavity. The longer the baseline of the interferometer, the longer the filter cavity needed. As such, it would become increasingly difficult to use external cavities. Fortunately, by using the interferometer itself as the filter cavity, the long baseline requirement for the filter cavity is naturally sufficed by the long baseline of the interferometer (because the are the same). In other words, using an EPR-based scheme that takes advantage of the dual role of the interferometer is naturally scalable to longer baselines. The figure below summarizes how to think of the full signal recycling cavity as a simple two-mirror filter cavity.
In our proposed EPR scheme, the achievable rotation angle is given as [25]

$$\Phi_{\text{rot}}^{\text{approx}} = \arctan\left(\frac{\Omega + \delta_f}{\gamma_f}\right) + \arctan\left(\frac{-\Omega + \delta_f}{\gamma_f}\right) \tag{1.109}$$

where δ_f and γ_f are the required detuning and bandwidth of the signal recycling interferometer with respect to the idler field, respectively [10, 26].

$$\gamma_f = \sqrt{\frac{128\omega_0 P_{\text{arm}}}{mc^2 T_{\text{SRC}}}} \tag{1.110}$$

$$\delta_f = -\gamma_f \tag{1.111}$$

From the definition of the signal recycling interferometer half bandwidth and the signal recycling cavity transmission given in [10, 24]

$$\gamma_f = \frac{c|T_{\text{SRC}}|}{4L_{\text{arm}}} \tag{1.112}$$

$$T_{\text{SRC}} = \frac{i\sqrt{T_{\text{SRM}}T_{\text{ITM}}}e^{2i\phi_{\text{SRC}}}}{(1 - \sqrt{R_{\text{ITM}}R_{\text{SRM}}}e^{2i\phi_{\text{SRC}}})} \tag{1.113}$$

we can derive

$$\gamma_f = \frac{T_{\text{SRM}}}{1 + R_{\text{SRM}}R_{\text{ITM}} - \sqrt{R_{\text{SRM}}R_{\text{ITM}}}\cos 2\phi_{\text{SRC}}} \tag{1.114}$$

We then equate this with Eq. (1.110) and solve for ϕ_{SRC}. This is the exact phase accumulated by the idler after one round trip in the SRC, so we denote it $\phi_{\text{SRC}}^{\text{exact}}$.

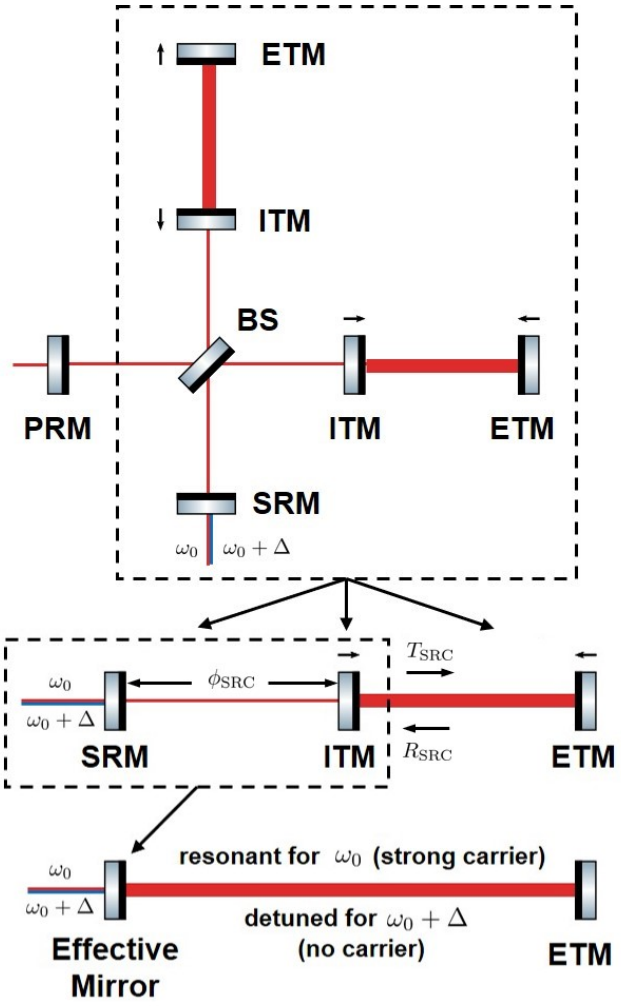

Figure 1.9: The signal recycling interferometer can be mapped to a three mirror cavity. The signal recycling cavity can then be mapped into a single mirror with an effective transmissivities and reflectivities [24]. This final, two-mirror cavity is resonant for the signal beam (at ω_0) but detuned for the idler beam (at $\omega_0 + \Delta$), thus the idler simply experiences a frequency-dependent ellipse rotation. That is, different off-resonant sidebands evolve under a free evolution governed by the field Hamiltonian (as described in Sec. 1.2.1). This allows us to use the interferometer itself as a filter cavity and to thus achieve broadband squeezing.

For our EPR squeezing scheme to work, we need to tune certain parameters to meet the following resonance condition

$$\begin{aligned} 2(\omega_{\text{idler}} + \delta_f)(\frac{L_{\text{arm}}}{c}) + \arg\left[R_{\text{SRC}}\right] &= 2n\pi \\ 2(\omega_0 + \Delta + \delta_f)(\frac{L_{\text{arm}}}{c}) + \arg\left[R_{\text{SRC}}\right] &= 2n\pi \\ 2(\Delta + \delta_f)(\frac{L_{\text{arm}}}{c}) + \arg\left[R_{\text{SRC}}\right] &= 2n\pi \end{aligned} \tag{1.115}$$

because $\omega_0 L/c = 2m\pi$ and where R_{SRC} is effective reflectivity of the signal recycling cavity and is given as

$$R_{\text{SRC}} = \frac{\sqrt{R_{\text{ITM}}} - \sqrt{R_{\text{SRM}}}e^{2i\phi_{\text{SRC}}}}{1 - \sqrt{R_{\text{ITM}}R_{\text{SRM}}}e^{2i\phi_{\text{SRC}}}} \tag{1.116}$$

So, we require $\delta_f = -\gamma_f$ and then tune the idler detuning, Δ, and $\phi_{\text{SRC}}^{\text{exact}}$ to find solutions to Eq. (1.115). Note that the tuned idler phase is denoted as $\phi_{\text{SRC}}^{\text{approx}}$. It is acceptable to tune this slightly from its exact value because the overall rotation angle is not very sensitive to changes in the SRC phase. Also note that Δ is given as

$$\Delta = \frac{(\phi_{\text{SRC}} + n\pi)c}{L} \tag{1.117}$$

so it is actually altered by tuning the integer parameter n, which tells us by how many free spectral ranges we shift the initial detuning. This is done to achieve a final detuning in the MHz regime.

The main arm length was proposed in the initial ET design study [5] to be around 10km, so we search for solutions where

$$L_{\text{arm}} \in [9995, 10000] \tag{1.118}$$

We search for signal recycling cavity lengths around those proposed in the Einstein Telescope design study [5]

$$L_{\text{SRC}} \in [100, 200] \tag{1.119}$$

The total idler detuning, Δ, has to be in the low Mhz regime because if it was lower it would interfere with the carrier, but if it were too high, electronics would not work optimally. The allowable range is taken to be

$$\frac{\Delta}{2\pi} \in [5, 50]\text{MHz or } \Delta \in [10\pi, 100\pi] \times 10^6\text{radians} \tag{1.120}$$

The minimum allowed detuning is 5MHz and this will occur when L_{SRC} is at its maximum, i.e. 200m. This will correspond to the minimum allowed n. From Eq. 1.117 we have

$$n_{\text{min}} = \frac{1}{\pi}(\frac{\Delta_{\text{min}} L_{\text{SRC,max}}}{c} - \phi_{\text{SRC}}) \approx 7 \tag{1.121}$$

We round to the nearest integer value. Similarly for the maximum allowed n

$$n_{\text{max}} = \frac{1}{\pi}(\frac{\Delta_{\text{max}} L_{\text{SRC,min}}}{c} - \phi_{\text{SRC}}) \approx 33 \tag{1.122}$$

We must search for integer values such that

$$n \in [7, 33] \tag{1.123}$$

The final tunable parameter is $\phi_{\rm SRC}^{\rm approx}$. We can sustain some error in the single trip phase the idler accumulates travelling through signal recycling cavity because the rotation angle is not highly sensitive to this phase. This makes it easier for us to find solutions to our resonance condition. As noted before, we must keep the error in the overall rotation angle to less than 0.02 rad. Mathematically, we need

$$|\Delta\Phi_{\rm rot}^{\rm approx}| < 0.02 \text{ rad} \tag{1.124}$$

where $\Delta\Phi_{\rm rot}^{\rm approx}$ is given in Eq. (1.109).

To linear order, the error in our rotation angle is related to the error in the signal recycling phase by

$$\Delta\Phi_{\rm rot}^{\rm approx} = \Delta\phi_{\rm SRC}\frac{d\Phi_{\rm rot}^{\rm approx}}{d\phi_{\rm SRC}} \tag{1.125}$$

We need to make sure that the error in rotation angle is less than 0.02rad over the whole positive frequency domain. Mathematically, we need

$$\max_{\Omega}|\Delta\phi_{\rm SRC}\frac{d\Phi_{\rm rot}^{\rm approx}}{d\phi_{\rm SRC}}| < 0.02 \tag{1.126}$$

Equivalently, because $\phi_{\rm SRC}$ is independent of Ω, we can write

$$|\Delta\phi_{\rm SRC}| < \frac{0.02}{\max_{\Omega}|\frac{d\Phi_{\rm rot}^{\rm approx}}{d\phi_{\rm SRC}}|} \tag{1.127}$$

Using Mathematica to differentiate Eq. (1.109) and using the given parameters for ET [5], one finds

$$|\Delta\phi_{\rm SRC}| < 0.002 \tag{1.128}$$

Thus, the domain of approximate phases is given as

$$\phi_{\rm SRC}^{\rm approx} \in [\phi_{\rm SRC}^{\rm exact} - 0.002, \phi_{\rm SRC}^{\rm exact} + 0.002] \tag{1.129}$$

Tunable Parameter	Domain	Step Size
$L_{\rm arm}$	[9995,10005]	1
$L_{\rm SRC}$	[100,200]	1
n	[7,33]	1
$\phi_{\rm SRC}^{\rm approx}$	$[\phi_{\rm SRC}^{\rm exact} - 0.002, \phi_{\rm SRC}^{\rm exact} + 0.002]$	0.0001

There are 1.2 million combinations of these parameters with the given step sizes. We took advantage of the fact that each combination is independent and can thus be checked in parallel. Our search resulted in **3444 working points** summarized in Fig. 1.10.

The step sizes were chosen with computational expense in mind, so the resolution is not particularly high. As such, Fig. 1.10 shows several "dead zones" as well as a couple "hot points". The natural question to ask is whether or not these are real or whether

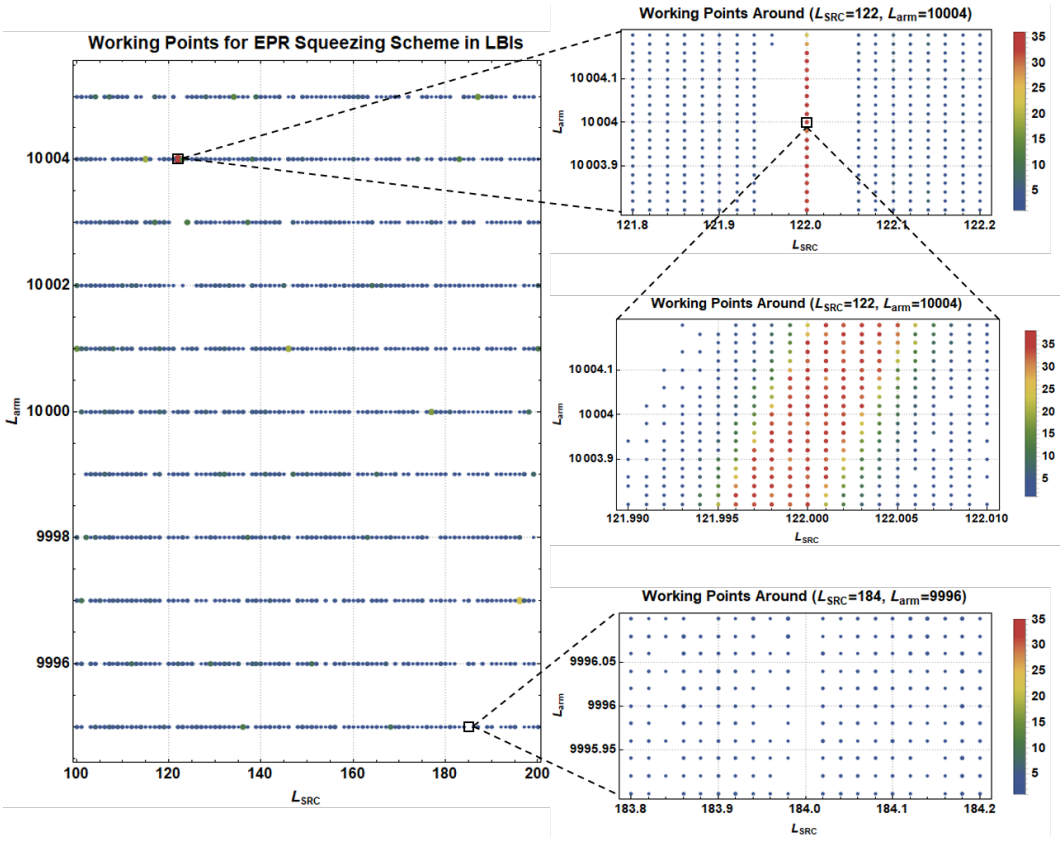

Figure 1.10: Working points of EPR squeezing scheme in ET. Each point represents a combination of the four tunable parameters for which the resonance condition was met. The color of the dot represents how many working points are at each combination of L_{SRC} and L_{arm}. For example, the red dot near the bottom right indicates there are 33 combinations of Δ and ϕ_{SRC}^{approx} for which the resonance condition was met when $L_{SRC} = 122m$ and $L_{arm} = 10,004m$

they are a byproduct of our numerical precision. Zooming in around two such points, we produced the subfigures on the righthand side of Fig. 1.10. In the case of the "dead zone", we see that there are actually working points where there appeared to be none. This is promising, as it points to the conclusion that a working point can be found given precise fine-tuning. Similarly, we zoomed in on a "hot point" (top right panel of Fig. 1.10) and interestingly we still see a line structure where there are as many as 35 working points surrounded by areas that apparently have zero working points. So, to check whether this was a real feature of the system or an issue of numerical precision, we again zoomed in round the "hot points." What we found, once again, is that the "dead zones" must be simply due to the numerical precision chosen. With more time or computational power (or both) one could map a relatively smooth landscape of working points for ET. In our case, our goal was to simply show that this EPR-based squeezing scheme is not very sensitive to the actual arm length and SRC length, and that we can always find some working points for given a set of parameters.

Using one of the many working points, we were able to plot the sensitivity of our approximate scheme alongside the exact scheme. It is clear from Fig. 1.11 that there is good agreement between the two. This is result of us heavily restricting our parameter space to bound the error.

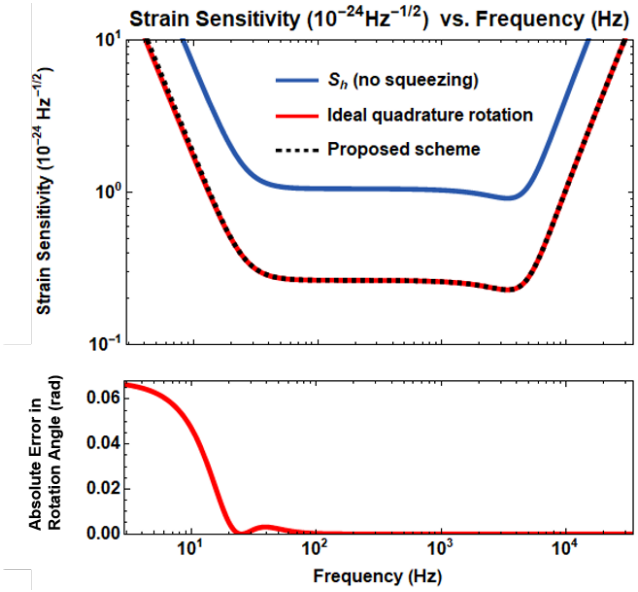

Figure 1.11: Top panel: square root of the single-sided noise power spectral density (sensitivity of the interferometer, dotted curve) plotted alongside the sensitivity when ideal ellipse rotation is achieved (top red curve). Bottom panel: Absolute value of the error between the ideal broadband squeezing scheme and our proposed EPR-based scheme. The absolute error is just the absolute value of the difference between the exact and approximate rotation angles.

1.5 Conclusions

We have shown that EPR entanglement-based squeezing can be implemented in LBIs. We derived the relevant bounds on the tunable parameters to ensure that our approximate ellipse rotation scheme very nearly matches the exact rotation achievable through the use of external filter cavities. The goal of the project was to map the interferometer working points for this squeezing scheme in LBIs like ET and Cosmic Explorer. We accomplished this at a rather low resolution of the parameter space. Zooming in around areas that had very many working points or very few showed that the landscape of working points seems to be quite smooth. In other words, if an area appears to have no working points, it is likely because the step size used to iterate through the parameter space was too low. This is good news for experimentalists, for if they cannot lock the interferometer at one exact spot, there should be another working point centimeters away. This result indicates the experimental feasibility of the scheme. We conclude that EPR-based squeezing is an appealing alternative to other broadband quantum noise reduction schemes that require additional filter cavities.

Chapter 2

Project 2: The Quantum Limits of Beam Displacement Measurements

2.1 Background and Introduction

Beam displacement measurements have been of interest to the quantum measurement community for several decades [27–29]. Because we deduce laws about the physical world through measurement, it is always desirable to be able to make more precise measurements. The natural question that arises is always: how well can we do? How precisely can we measure something given a certain set-up. Answering this question is the theme of this project.

Specifically, we calculate the signal-to-noise ratio (SNR) for various beam displacement detection schemes. Our goal was to determine which detector could more effectively measure a deflected TEM00 beam: a split detector (SD) or a position sensitive detector (PSD). The latter does not appear to have been treated quantum mechanically in the literature. Thus, to the best of our knowledge, our result is novel and of interest to anyone attempting to measure the displacement of a laser beam with great precision.

There are many applications for the precise measurement of beam displacements. The application most often mentioned is atomic force microscopy (AFM) readout. In an AFM, a stylus scans over a material and receives a time-varying force. This force raises or lowers the stylus and deflects the laser beam impinging on it. The detection of this deflection limits the resolution of the AFM. Thus, with higher SNRs in the AFM readout, one could achieve higher resolution AFMs.

We first review the analysis of linear interferometers and split detectors laid out by Barnett et al. [27]. Having learned the methods of analysis from them, we make small improvements to their technique and show how the calculation for both the split detector and the position sensitive detectors can be treated almost identically, by using what we call a "detector response function." Finally, we show that the PSD should have a standard

quantum limit (SQL) of about 2dB below that of the SD. We then show that this is expected when one examines the so-called Quantum Cramer-Rao Bound (QCRB) for the system.

2.2 Linear Interferometer

We first derive the sensitivity of a simple Michelson interferometer following the analysis laid out by Barnett et. al. [27].

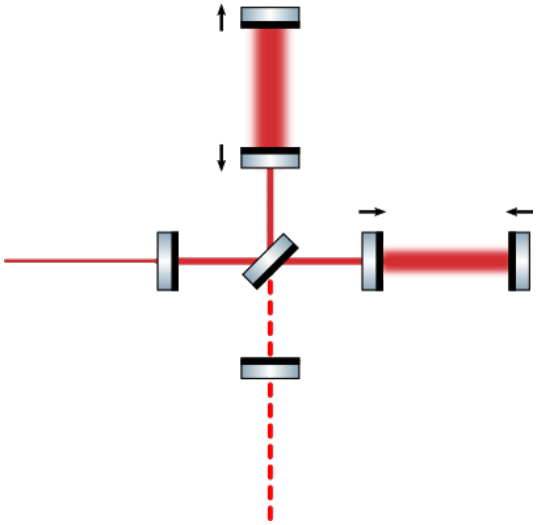

Figure 2.1: A simple Michelson interferometer.

A Michelson-type interferometer has an input-output relation given as

$$\hat{a}_{\text{out}} = \cos\left(\frac{\phi}{2}\right)\hat{a} + \sin\left(\frac{\phi}{2}\right)\hat{b} \tag{2.1}$$

$$\hat{b}_{\text{out}} = \cos\left(\frac{\phi}{2}\right)\hat{b} - \sin\left(\frac{\phi}{2}\right)\hat{a} \tag{2.2}$$

where ϕ is the relative phase between the two arms. If the two arms are perfectly in phase ($\phi = 0$), then $\hat{a}_{\text{out}} = \hat{a}$ and $\hat{b}_{\text{out}} = \hat{b}$. If they are fully out of phase ($\phi = \pi$), then $\hat{a}_{\text{out}} = \hat{b}$ and $\hat{b}_{\text{out}} = \hat{a}$. Any intermediate configuration gives some linear combination of the two fields, as expected. Where, as above, we are working in the Heisenberg picture and doing calculations on the creation and annihilation operators associated with certain modes of the quantized electromagnetic field. More on this in the next section, where we begin to discuss the SQL.

2.2.1 Standard Quantum Limit

Roy J. Glauber established the theory of optical coherence over 50 years ago [30]. In his seminal paper, he showed that the photocurrent produced by a photodiode should be proportional to the quantity $\langle \psi^{(-)}\psi^{(+)} \rangle$ where $\psi^{(+)}$ is the optical field impinging on the

photodiode. Thus, any time we wish to calculate a signal from a photodetector, we should calculate this expectation value. However, it turns out that the above quantity is always proportional to $\langle \hat{a}^\dagger \hat{a} \rangle$ where $\hat{a}$ is the creation operator for your quantized electromagnetic field. Recall, that the creation and annihilation operators replace the complex amplitudes in the classical description of an electromagnetic field. We often refer to the operator $\hat{a}$ as a mode of the electromagnetic field when in fact it is more precise to say that it is the creation operator associated with a mode of the quantized electromagnetic field. Where a mode is simply a normalized solution to Maxwell's equations in free space. See Ref. [16] for a great review about modes and states in quantum optics. For our purposes, it suffices to say that in the Heisenberg picture, it is easier to use the creation and annihilation operators when doing direct detection calculations, rather than the full field operator. As we will see in later sections, though, sometimes the first principles approach is required. With all this in mind, we should feel comfortable writing the signal of an interferometer with direct readout as the difference in photon number at the two output ports

$$\begin{aligned} \text{Signal} &= \langle \hat{a}^\dagger_{\text{out}} \hat{a}_{\text{out}} - \hat{b}^\dagger_{\text{out}} \hat{b}_{\text{out}} \rangle && (2.3) \\ &= \langle (\hat{a}^\dagger \hat{a} - \hat{b}^\dagger \hat{b}) \cos(\phi) + (\hat{a}^\dagger \hat{b} + \hat{b}^\dagger \hat{a}) \sin(\phi) \rangle && (2.4) \end{aligned}$$

The signal when one arm gets a tiny ($\Delta\phi << 1$) phase shift, is

$$\text{Signal} = \langle (\hat{a}^\dagger \hat{a} - \hat{b}^\dagger \hat{b}) \cos(\phi + \Delta\phi) + (\hat{a}^\dagger \hat{b} + \hat{b}^\dagger \hat{a}) \sin(\phi + \Delta\phi) \rangle \quad (2.5)$$

The SQL is reached, by definition, when one input is prepared in a coherent state and the other is left in a vacuum state. Here, we have the field represented by the operator $\hat{a}$ in a coherent state, $|\alpha\rangle$, and the field associated with $\hat{b}$ in a vacuum state, $|0\rangle$. With this, the signal becomes

$$\text{Signal} = |\alpha|^2 \cos(\phi + \Delta\phi) \quad (2.6)$$

because $\hat{a}|\alpha\rangle = \alpha, \langle\alpha|\hat{a}^\dagger = \alpha^*$, and $\hat{b}|0\rangle = 0$.

We wish to operate the interferometer such that it is as sensitive as possible to small changes in phase. In other words, we need to find where the slope of the signal achieves a maximum. This is equivalent to finding the inflection points of the signal by taking two derivatives with respect to $\Delta\phi$ and setting that expression equal to zero

$$\frac{\partial^2}{\partial \Delta\phi^2}[\text{Signal}] = -|\alpha|^2 \cos(\phi + \Delta\phi) = 0 \quad (2.7)$$

This is true when $\phi = \pm\pi/2$ (remember, we assume $\Delta\phi << 1$). We choose $\phi = -\pi/2$ so we have a positive signal slope. With this working point and focusing on small phase shifts (so that we can use a first order Taylor expansion of the sinusoid) we find

$$\begin{aligned} \text{Signal} &= |\alpha|^2 \cos(-\pi/2 + \Delta\phi) && (2.8) \\ &= |\alpha|^2 \sin(\Delta\phi) && (2.9) \\ \text{Signal} &\approx |\alpha|^2 \Delta\phi && (2.10) \end{aligned}$$

The noise is set by the square root of the variance of whatever Hermitian operator represents the signal (in our case this is the photon number difference operator from Eq.

(**??**)). Note that this variance is calculated without any phase shift, so setting $\Delta\phi = 0$ and $\phi = \pi/2$, we get

$$\text{Variance} = \langle(\hat{a}^\dagger_{\text{out}}\hat{a}_{\text{out}} - \hat{b}^\dagger_{\text{out}}\hat{b}_{\text{out}})^2\rangle - \langle\hat{a}^\dagger_{\text{out}}\hat{a}_{\text{out}} - \hat{b}^\dagger_{\text{out}}\hat{b}_{\text{out}}\rangle^2 \tag{2.11}$$

$$= \langle(\hat{a}^\dagger_{\text{out}}\hat{a}_{\text{out}} - \hat{b}^\dagger_{\text{out}}\hat{b}_{\text{out}})^2\rangle \tag{2.12}$$

$$= \langle\hat{a}^\dagger\hat{b}\hat{a}^\dagger\hat{b} + \hat{a}^\dagger\hat{b}\hat{b}^\dagger\hat{a} + \hat{b}^\dagger\hat{a}\hat{a}^\dagger\hat{b} + \hat{b}^\dagger\hat{a}\hat{b}^\dagger\hat{a}\rangle \tag{2.13}$$

Eq. (2.11) is the general variance expression for this working point. The standard quantum limit is reached when mode a is in a coherent state and mode b in a vacuum state. In this case, the variance is simply

$$\text{Variance} = |\alpha|^2 \tag{2.14}$$

The noise is set by the square root of this expression. Thus, the signal-to-noise ratio (SNR), where $|\alpha|^2 = N$ is the mean number of photons is

$$\frac{\text{Signal}}{\text{Noise}} = N^{1/2}\Delta\phi \tag{2.15}$$

The minimum resolvable phase shift occurs when the SNR equals one. Thus, we have

$$\Delta\phi = N^{-1/2} \tag{2.16}$$

This is the SQL of detecting a small phase shift using a linear Michelson interferometer.

2.2.2 Surpassing the SQL

We can surpass the SQL by preparing mode b in a squeezed vacuum state. We make the simplifying assumption that the mirrors are infinitely massive, thus radiation pressure forces from the light will not add noise to our system. Thus, the limiting noise source is quantum shot noise. This noise can be thought of in several different ways, but here we think of it as uncertainty in the phase quadrature of the quantized electromagnetic field which affects the statistical distribution of the photon number difference and thus weakens the interferometer's ability to estimate phase. Thus, to reduce this noise we prepare mode b in a phase-squeezed vacuum state. A single-mode squeezed vacuum state is written as

$$|\Psi_b\rangle = |\xi\rangle = \hat{S}\,|0\rangle = e^{(-\xi\hat{a}^{\dagger 2} + \hat{a}^2\xi^*)/2}\,|0\rangle \tag{2.17}$$

where $\xi = re^{2i\theta_s}$, r is the squeezing factor that defines the strength of your squeezer, and θ_s is the squeezing angle that defines what quadrature your are squeezing. In our case, we need a phase-squeezed vacuum state, so we will set $\theta_s = 0$. Practically speaking, one only needs to know how the phase squeezing operator transforms our creation and annihilation operators. The relevant transformations are

$$\hat{S}^\dagger\hat{b}\hat{S} = \hat{b}\cosh r - \hat{b}^\dagger\sinh r \tag{2.18}$$

$$\hat{S}^\dagger\hat{b}^\dagger\hat{S} = \hat{b}^\dagger\cosh r - \hat{b}\sinh r \tag{2.19}$$

From Eq. (2.5) above, we know that our signal is most generally written as

$$\text{Signal} = \langle(\hat{a}^\dagger\hat{a} - \hat{b}^\dagger\hat{b})\cos(\phi + \Delta\phi) + (\hat{a}^\dagger\hat{b} + \hat{b}^\dagger\hat{a})\sin(\phi + \Delta\phi)\rangle \tag{2.20}$$

Now letting $\phi = -\pi/2$ and $\Delta\phi << 1$ as before, our signal becomes a first order approximation of Eq. (2.5)

$$\text{Signal} = \langle(\hat{a}^\dagger\hat{a} - \hat{b}^\dagger\hat{b})\Delta\phi - (\hat{a}^\dagger\hat{b} + \hat{b}^\dagger\hat{a})\rangle \tag{2.21}$$

We now assume mode a is in a strong coherent state which can be approximated as a classical field amplitude such that $\hat{a} \approx \alpha = |\alpha|e^{i\theta}$ where $\theta = \arg(\alpha)$. The signal becomes

$$\text{Signal} = \Delta\phi(|\alpha|^2 - \langle\hat{b}^\dagger\hat{b}\rangle) - |\alpha|\langle\hat{b}e^{-i\theta} + \hat{b}^\dagger e^{i\theta}\rangle \tag{2.22}$$

Now to update the variance, we return to Eq. (2.11)

$$\text{Variance} = \langle\hat{a}^\dagger\hat{b}\hat{a}^\dagger\hat{b} + \hat{a}^\dagger\hat{b}\hat{b}^\dagger\hat{a} + \hat{b}^\dagger\hat{a}\hat{a}^\dagger\hat{b} + \hat{b}^\dagger\hat{a}\hat{b}^\dagger\hat{a}\rangle \tag{2.23}$$

$$= \langle\hat{a}^\dagger\hat{b}\hat{a}^\dagger\hat{b} + \hat{a}^\dagger\hat{b}\hat{b}^\dagger\hat{a} + \hat{b}^\dagger(1 + \hat{a}^\dagger\hat{a})\hat{b} + \hat{b}^\dagger\hat{a}\hat{b}^\dagger\hat{a}\rangle \tag{2.24}$$

The only difference between the above lines is that we have used the boson commutation relation for the creation and annihilation operator $[\hat{a}, \hat{a}^\dagger] = 1$. This so-called *normal ordering* was not needed before because mode b was in a vacuum state and thus most terms went to zero. With this change made, and remembering that we are approximating mode a as a classical field, we find a variance of

$$\text{Variance} = \langle|\alpha|^2 e^{-2i\theta}\hat{b}^2 + |\alpha|^2 e^{2i\theta}\hat{b}^{\dagger 2} + |\alpha|^2\hat{b}\hat{b}^\dagger + \hat{b}\hat{b}^\dagger + |\alpha|^2\hat{b}^\dagger\hat{b}\rangle \tag{2.25}$$

$$= |\alpha|^2\langle(\hat{b}e^{-i\theta} + \hat{b}^\dagger e^{i\theta})^2\rangle + \langle\hat{b}^\dagger\hat{b}\rangle \tag{2.26}$$

So, we see that the variance depends on the uncertainty in vacuum field entering the interferometer. It is these so-called vacuum fluctuations that limit the sensitivity of an interferometer. Specifically, we are saying that the variance in the quadrature operators of the field associated with the $\hat{b}$ operator limits the sensitivity of the interferometer. Recall that the amplitude and phase quadratures are proportional to $\hat{b} + \hat{b}^\dagger$ and $i(\hat{b} - \hat{b}^\dagger)$, respectively. The exact normalization differs between sources but the crucial point is that these quadratures are observable quantities analogous to the amplitude and phase of classical light. In this case, the quantum fluctuations in the phase quadrature limit the sensitivity of our detector.

To surpass the SQL, we let $\theta = 0$ in Eq. (2.24) and prepare b in an phase-squeezed vacuum state. With these changes our variance becomes

$$\text{Variance} = |\alpha|^2\langle(\hat{b} + \hat{b}^\dagger)^2\rangle + \langle\hat{b}^\dagger\hat{b}\rangle \tag{2.27}$$

$$= |\alpha|^2\langle\hat{b}\hat{b} + \hat{b}\hat{b}^\dagger + \hat{b}^\dagger\hat{b} + \hat{b}^\dagger\hat{b}^\dagger\rangle + \langle\hat{b}^\dagger\hat{b}\rangle \tag{2.28}$$

$$= |\alpha|^2\langle\xi|\,\hat{b}\hat{b} + \hat{b}\hat{b}^\dagger + \hat{b}^\dagger\hat{b} + \hat{b}^\dagger\hat{b}^\dagger\,|\xi\rangle + \langle\xi|\,\hat{b}^\dagger\hat{b}\,|\xi\rangle \tag{2.29}$$

Using the fact that $|\xi\rangle = \hat{S}|0\rangle$, $\hat{S}\hat{S}^\dagger = \hat{I}$, and the transformations of the creation and annihilation operators given above we get

$$\begin{aligned}\text{Variance} &= |\alpha|^2\langle 0|\,\hat{S}^\dagger\hat{b}\hat{S}\hat{S}^\dagger\hat{b}\hat{S} + \hat{S}^\dagger\hat{b}\hat{S}\hat{S}^\dagger\hat{b}^\dagger\hat{S} \\ &\quad + \hat{S}^\dagger\hat{b}^\dagger\hat{S}\hat{S}^\dagger\hat{b}\hat{S} + \hat{S}^\dagger\hat{b}^\dagger\hat{S}\hat{S}^\dagger\hat{b}^\dagger\hat{S}\,|0\rangle + \langle 0|\,\hat{S}^\dagger\hat{b}^\dagger\hat{S}\hat{S}^\dagger\hat{b}\hat{S}\,|0\rangle \\ &= |\alpha|^2 e^{-2r} + \sinh^2 r\end{aligned} \tag{2.30}$$

where we note that $\langle\hat{b}^\dagger\hat{b}\rangle$ is the expected number of photons in mode b which is in a squeezed vacuum state. It is interesting and slightly counterintuitive that there is a nonzero expected

number of photons in a squeezed vacuum (given that vacuum is a term that is associated with nothingness, etc). The signal to noise ratio is then given as

$$\text{SNR} = \frac{\Delta\phi(|\alpha|^2 - \sinh^2 r)}{(|\alpha|^2 e^{-2r} + \sinh^2 r)^{1/2}} \tag{2.31}$$

While in the low squeezing regime, we assume $|\alpha|^2 >> \sinh^2 r$ thus our SNR becomes

$$\text{SNR} \approx \frac{\Delta\phi|\alpha|^2}{|\alpha|e^{-r}} = \Delta\phi N^{1/2} e^r \tag{2.32}$$

where $|\alpha|^2 \approx N$. Setting this expression equal to one we can solve for the minimum resolvable phase shift

$$\Delta\phi = \frac{1}{N^{1/2} e^r} \tag{2.33}$$

Thus we surpass the SQL by a factor of e^r. We must note, however, that we have made some crucial simplifying assumptions. Primarily, the assumption that the coherent field is strong enough to be treated as a classical field is a big assumption. This analysis would hold well in an infinite energy limit of the coherent field. Of course, at finite energies, the quantum nature of the coherent field would need to be taken into account. Moreover, we assume infinitely massive mirrors – an assumption that may not hold depending on the power regime and mirror properties. Nonetheless, the analysis gives a nice, simple introduction to the concept of the SQL and how squeezed light can be used to surpass it. We now turn to our next detector: the split detector.

2.3 Split Detector in Single-mode Regime

We will now analyze the performance of a split detector. A split detector is simply a segmented photodiode wired such that the photocurrent produced on one side is subtracted from the photocurrent produced on the other after some amplification. The detector re-

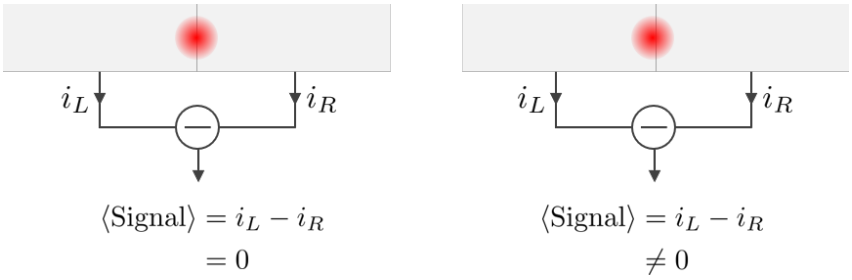

Figure 2.2: Schematic of a split detector with impinging beam with Gaussian beam profile. Left: beam is centered perfectly on the detector and the expected current difference is zero. Right: a slightly displaced beam gives rise to a difference in photocurrents. This acts as our signal.

sponse function, which we denote $\Theta(x)$, is simply a step function. What is actually measured depends on the light impinging on the detector. Thus, the detector mode is the detector response function multiplied by the beam profile. In the case of the split detector, the detector mode is a flipped Gaussian. A flipped Gaussian is just the product between a step

function and a normal Gaussian. The step function causes the Gaussian to "flip" at $x = 0$ as shown in Fig. 2.3

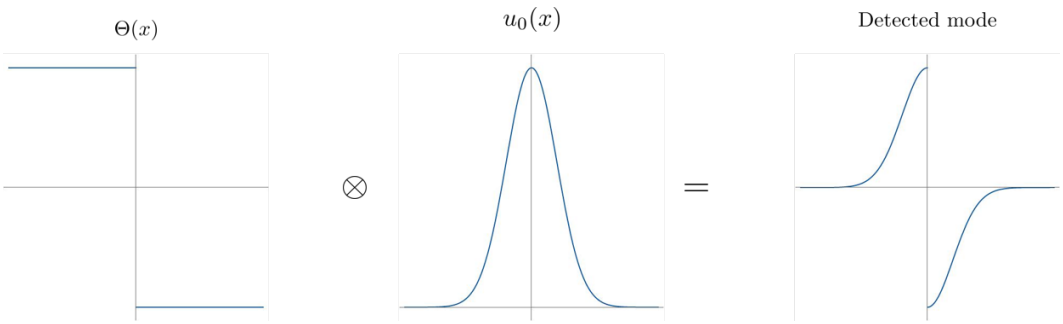

Figure 2.3: Visualization of the detector mode times the transverse optical mode, which yields the detected mode.

Here we formally derive the signal to noise ratio when either zero or one spatial mode is squeezed. Unlike Barnett et al. [27], we encode the beam displacement information in the coherent state of light. This is a general method that can be utilized in other beam displacement detector set-ups.

2.3.1 Deflected Coherent State

Let $\hat{a}(x, y)$ denote a field annihilation operator associated with the point (x,y) in space and $u_i(x, y)$ be the i^{th} basis mode function. Our field is given as

$$\hat{\psi}^{(+)}(x, y) = \sum_i^n u_i(x, y)\hat{a}(x, y) \tag{2.34}$$

which, because $\int\int u_i^* u_j dxdy = \delta_{ij}$ implies

$$\hat{a}_i = \int\int u_i^*(x, y)\hat{\psi}^{(+)}(x, y)dxdy \tag{2.35}$$

This is analogous to the decomposition of the classical electromagnetic field with complex amplitudes replaced by bosonic creation/annihilation operators as mentioned in the previous project. A fine review of modes and states in qauntum optics is given in Ref. [16]. Here we have the decomposition of our transverse beam profile into an orthogonal set of spatial modes. Our initial quantum state is described as

$$|\Psi\rangle = |\alpha\rangle_0 \otimes |0\rangle_1 \otimes |0\rangle_2 \otimes \dots \tag{2.36}$$

where the subscript makes explicit what mode to which we are referring. We model the small displacement using a unitary operator, $\hat{U}_0(\theta)$ (where θ is a small distance) such that

$$|\Psi(\theta)\rangle = \hat{U}_0(\theta)\,|\Psi\rangle \tag{2.37}$$

$$= \hat{U}_0(\theta)\,|\alpha\rangle_0 \otimes |0\rangle_1 \otimes |0\rangle_2 \otimes \dots \tag{2.38}$$

$$= \hat{U}_0(\theta)e^{\alpha\hat{a}_0^\dagger - \alpha^*\hat{a}_0}\,|0\rangle_0 \otimes |0\rangle_1 \otimes |0\rangle_2 \otimes \dots \tag{2.39}$$

$$= \hat{U}_0(\theta)e^{\alpha\hat{a}_0^\dagger - \alpha^*\hat{a}_0}\hat{U}_0^\dagger(\theta)\,|0\rangle_0 \otimes |0\rangle_1 \otimes |0\rangle_2 \otimes \dots \tag{2.40}$$

Now, expanding the exponential in Eq. (2.40) and multiplying by the operator on either side, we would get

$$|\Psi(\theta)\rangle = e^{\alpha \hat{U}_0(\theta)\hat{a}_0^\dagger \hat{U}_0^\dagger(\theta) - \alpha^* \hat{U}_0(\theta)\hat{a}_0 \hat{U}_0^\dagger(\theta)} |0\rangle_0 \otimes |0\rangle_1 \otimes |0\rangle_2 \otimes \dots \tag{2.41}$$

Our new state will be determined once we work out the transformations on our creation and annihilation operators. From our definitions, we have

$$\begin{aligned} \hat{U}(\theta)\hat{a}_0\hat{U}^\dagger(\theta) &= \int\int u_0^*(x,y)\hat{U}(\theta)\hat{\psi}^{(+)}(x,y)\hat{U}^\dagger(\theta)dxdy \\ &= \int\int u_0(x,y)\hat{\psi}^{(+)}(x-\theta,y)dxdy \end{aligned} \tag{2.42}$$

Letting $x' = x - \theta$ and then expanding the mode function to first order in θ (that is, we are dropping higher order terms in the Taylor expansion because we assume the displacement is very small) we can write

$$\begin{aligned} \hat{U}(\theta)\hat{a}_0\hat{U}^\dagger(\theta) &= \int\int u_0(x'+\theta,y)\hat{\psi}^{(+)}(x',y)dx'dy \\ &= \int\int (u_0(x',y) + \theta u_0'(x',y))\hat{\psi}^{(+)}(x',y)dx'dy \end{aligned} \tag{2.43}$$

Now, $u_0'(x,y)$ is not dimensionally consistent with or orthonormal to $u_0(x,y)$. Meaning, when we take the spatial derivative of our mode, the dimension changes. If we wish to use the derivative of the zeroth mode as another element of our basis, we must work out the proportionality constant that will allow us to remain dimensionally consistent and to maintain the orthonormality of our mode basis. Let's call the function we seek u_1. It is given as

$$u_1(x',y) = Bx\left(e^{-\frac{x'^2+y^2}{2w_0^2}}\right) \tag{2.44}$$

To ensure normalization we integrate over all space and set the integral equal to one. This allows us to solve for B. The resultant mode function is given as

$$u_1(x',y) = -\sqrt{\frac{2}{\pi}}\frac{x'}{w_0^2}\left(e^{-\frac{x'^2+y^2}{2w_0^2}}\right) \tag{2.45}$$

One can then derive $u_0'(x',y)$ by differentiating with respect to x

$$u_0 = \frac{1}{\sqrt{\pi}w_0}e^{-\frac{x^2+y^2}{2w_0^2}} \tag{2.46}$$

$$u_0'(x',y) = -\frac{x'e^{-\frac{x'^2+y^2}{2w_0^2}}}{\sqrt{\pi}w_0^3} \tag{2.47}$$

We see that $u_0'(x',y) = \frac{u_1(x',y)}{\sqrt{2}w_0}$. Making this substitution to equation

$$\begin{aligned} \hat{U}(\theta)\hat{a}_0\hat{U}^\dagger(\theta) &= \int\int (u_0(x',y) + \theta\frac{u_1(x',y)}{\sqrt{2}w_0})\hat{\psi}^{(+)}(x',y)dx'dy \\ &= \hat{a}_0 + \frac{\theta}{\sqrt{2}w_0}\hat{a}_1 \end{aligned} \tag{2.48}$$

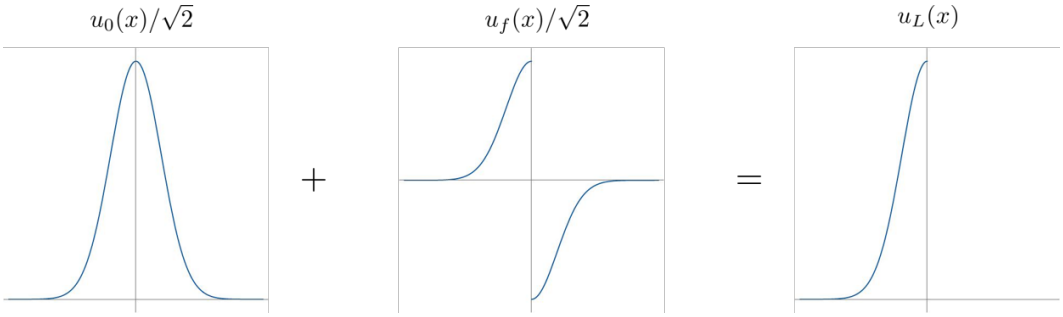

Figure 2.4: We break the modes into an even and flipped Gaussians to simplify the calculation.

The daggered expression is identical (but with creation instead of annihilation operators). Substituting these into Eq. (2.41) gives

$$|\Psi(\theta)\rangle = e^{\alpha(\hat{a}_0^\dagger + \frac{\theta}{\sqrt{2}w_0})\hat{a}_1^\dagger - \alpha^*(\hat{a}_0 + \frac{\theta}{\sqrt{2}w_0}\hat{a}_1)} |0\rangle_0 \otimes |0\rangle_1 \otimes |0\rangle_2 \otimes \dots \tag{2.49}$$

Rearranging we find

$$|\Psi(\theta)\rangle = |\alpha\rangle_0 \otimes |\frac{\theta\alpha}{\sqrt{2}w_0}\rangle_1 \otimes |0\rangle_2 \otimes |0\rangle_3 \dots \tag{2.50}$$

Because the displacement is small, it is sufficient to focus only on first order in θ (where again, θ represents our small displacement). Thus, we have chosen a basis in which the deflection excites the first mode and the higher order modes are left approximately in vacuum states. This would not hold for large displacements. To first order, we see that our state now depends on the small displacement, as desired.

2.3.2 Standard Quantum Limit

Following the definitions in Barnett et. al. [27], we introduce the flipped Gaussian $u_f \equiv u_0 \text{sign}(x)$. This differs slightly from their notation, in which they had an even and odd mode denoted u_e and u_o, respectively. The mode to which the left side of the split detector is sensitive is then given as

$$u_\text{L} = \frac{1}{\sqrt{2}}(u_0 + u_f) \tag{2.51}$$

and the right side of the split detector sees

$$u_\text{R} = \frac{1}{\sqrt{2}}(u_0 - u_f) \tag{2.52}$$

The creation operators for these modes have the same form

$$\hat{a}_\text{L} = \frac{1}{\sqrt{2}}(\hat{a}_0 + \hat{a}_f) \tag{2.53}$$

$$\hat{a}_\text{R} = \frac{1}{\sqrt{2}}(\hat{a}_0 - \hat{a}_f) \tag{2.54}$$

These modes can be thought of as "what the detector sees" and will make our calculation of the signal-to-noise ratio far simpler than working from the definition of our field in Eq.

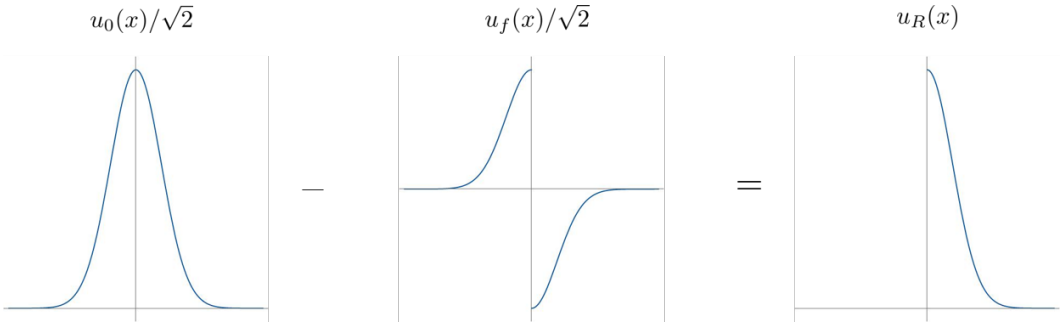

Figure 2.5: We break the modes into an even and flipped Gaussians to simplify the calculation.

(2.34). Now, assuming perfect photodiodes, the split detector's signal will simply be the difference in the number of photons impinging on the left and right photodiode

$$\langle \hat{N}_{\mathrm{L}} \rangle - \langle \hat{N}_{\mathrm{R}} \rangle = \langle \hat{a}_{\mathrm{L}}^{\dagger} \hat{a}_{\mathrm{L}} - \hat{a}_{\mathrm{R}}^{\dagger} \hat{a}_{\mathrm{R}} \rangle \tag{2.55}$$

$$= \langle \frac{1}{2}(\hat{a}_0^{\dagger} + \hat{a}_f^{\dagger})(\hat{a}_0 + \hat{a}_f) - \frac{1}{2}(\hat{a}_0^{\dagger} - \hat{a}_f^{\dagger})(\hat{a}_0 - \hat{a}_f) \rangle \tag{2.56}$$

$$= \langle \hat{a}_0^{\dagger} \hat{a}_f + \hat{a}_f^{\dagger} \hat{a}_0 \rangle \tag{2.57}$$

In order to act on the state that is given in Eq. (2.50), we need to find out what $\hat{a}_f$ is in terms of the mode basis used to calculate the state. To do so, we return to the definition in Eq. (2.35)

$$\hat{a}_f = \int_{-\infty}^{+\infty} \int_{-\infty}^{+\infty} u_f^* \hat{\psi}^{(+)}(x,y) dx dy \tag{2.58}$$

$$= \int_{-\infty}^{+\infty} \int_{-\infty}^{+\infty} u_f^* [\hat{a}_0 u_0 + \hat{a}_1 u_1 + \dots] dx dy \tag{2.59}$$

$$= \int_{-\infty}^{+\infty} \int_{-\infty}^{+\infty} \hat{a}_1 u_f^* u_1 + \hat{a}_3 u_f^* u_3 + \dots dx dy \tag{2.60}$$

where the last equality holds because $u_f \times$(any even mode) integrates to zero over all space. Now, the remaining terms are even because $u_f \times$(any odd mode) is even thus we use the fact that

$$\int_{-\infty}^{+\infty} (\text{even function}) dx = 2 \int_{0}^{+\infty} (\text{even function}) dx \tag{2.61}$$

Moreover, we use the fact that $u_f = -u_0$ from $0 \to \infty$ and that all modes other than $\hat{a}_1$ are in vacuum. Using all these facts we arrive at the expression

$$\hat{a}_f = -2 \int_{-\infty}^{+\infty} \int_{0}^{+\infty} \hat{a}_1 u_0 u_1 dx dy \tag{2.62}$$

$$= -2 \int_{-\infty}^{+\infty} \int_{0}^{+\infty} \hat{a}_1 \left(\frac{1}{\sqrt{\pi} w_0} e^{-\frac{x^2+y^2}{2w_0^2}} \right) \left(-\sqrt{\frac{2}{\pi}} \frac{x}{w_0^2} \left(e^{-\frac{x^2+y^2}{2w_0^2}} \right) \right) dx dy \tag{2.63}$$

$$\hat{a}_f = \sqrt{\frac{2}{\pi}} \hat{a}_1 \tag{2.64}$$

Returning to our original signal expression

$$\langle \hat{N}_{\mathrm{L}} \rangle - \langle \hat{N}_{\mathrm{R}} \rangle = \langle \hat{a}_0^\dagger \hat{a}_f + \hat{a}_f^\dagger \hat{a}_0 \rangle \tag{2.65}$$

$$= \langle \hat{a}_0^\dagger \sqrt{\frac{2}{\pi}} \hat{a}_1 + \sqrt{\frac{2}{\pi}} \hat{a}_1^\dagger \hat{a}_0 \rangle \tag{2.66}$$

$$= \langle \alpha, \frac{\theta\alpha}{\sqrt{2}w_0} | \, \hat{a}_0^\dagger \sqrt{\frac{2}{\pi}} \hat{a}_1 + \sqrt{\frac{2}{\pi}} \hat{a}_1^\dagger \hat{a}_0 \, | \alpha, \frac{\theta\alpha}{\sqrt{2}w_0} \rangle \tag{2.67}$$

$$= \alpha^* \sqrt{\frac{2}{\pi}} \frac{\theta}{\sqrt{2}} w_0 \alpha + \alpha^* \sqrt{\frac{2}{\pi}} \frac{\theta}{\sqrt{2}} w_0 \alpha \tag{2.68}$$

$$= \frac{2\theta|\alpha|^2}{\sqrt{\pi} w_0} \tag{2.69}$$

$$\text{Signal} = \frac{2N}{\sqrt{\pi} w_0} \Delta x \tag{2.70}$$

The noise is the square root of the variance for the photon number difference operator. That is,

$$\text{Noise} = \sqrt{\mathrm{Var}(\hat{N}_-)} \tag{2.71}$$

$$= \sqrt{\langle \hat{N}_- \rangle} \tag{2.72}$$

To first order, the noise for the displacement measurement is determined by the photon shot noise of the undisplaced beam. This means no higher order modes have been excited and we model the laser as a coherent state. Thus, the state we calculate the expectation values with respect to is a coherent state in the zeroth mode (associated with $\hat{a}_0$) and vacuum in all other modes.

$$|\psi\rangle = |\alpha\rangle \otimes |0\rangle \otimes \dots \tag{2.73}$$

The result is just the variance of a coherent state. Because the coherent state has Poissonian statistics, we know that the variance is equal to the mean (always true for a coherent state). In short,

$$\text{Noise} = \sqrt{N} \tag{2.74}$$

Thus, our SNR is

$$\text{SNR} = \frac{2\Delta x}{\sqrt{\pi} w_0} \sqrt{N} \tag{2.75}$$

Note that this SNR scales as $\sqrt{N}$ just as the homodyne detection for a normal interferometer. There is actually a rather subtle connection between these two measurement techniques. In fact, one can imagine a split detection measurement as a homodyne measurement of mode u_1 using u_0 as a local oscillator. This is one way to understand the similar scaling of SNR.

2.3.3 Detector Response Method

We will now derive the exact same SNR using a new method that is more general. This will then allow us to very easily compare the SD to the PSD. In this new method, our signal is given as

$$\text{Signal} = \langle \int_{-\infty}^{\infty} \int_{-\infty}^{\infty} \Theta(x) \psi^{(-)} \psi^{(+)} dx dy \rangle \tag{2.76}$$

where $\Theta(x)$ is our detector response function and our optical field is decomposed as $\psi^{(+)} = u_0\hat{a}_0 + u_1\hat{a}_1 + \sum_i u_i\hat{a}_i$. Where all the modes with $i > 1$ are in vacuum, therefor $\langle \hat{a}_i^\dagger \hat{a}_i \rangle = 0$. So, we have

$$\text{Signal} = \langle \int_{-\infty}^{\infty}\int_{-\infty}^{\infty} \Theta(x)(u_0u_0\hat{a}_0^\dagger\hat{a}_0 + u_0u_1\hat{a}_0^\dagger\hat{a}_1 + u_1u_0\hat{a}_1^\dagger\hat{a}_0 + u_1u_1\hat{a}_1^\dagger\hat{a}_1)dxdy\rangle \tag{2.77}$$

Now we can use the fact that the response function, $\Theta(x)$, is a step function and break the integral into two

$$\text{Signal} = \langle \int_{-\infty}^{\infty}\int_{-\infty}^{\infty} \Theta(u_0u_0\hat{a}_0^\dagger\hat{a}_0 + u_0u_1\hat{a}_0^\dagger\hat{a}_1 + u_1u_0\hat{a}_1^\dagger\hat{a}_0 + u_1u_1\hat{a}_1^\dagger\hat{a}_1)dxdy\rangle \tag{2.78}$$

$$\text{Signal} = \langle \int_{-\infty}^{\infty}\int_{-\infty}^{0} -(u_0u_0\hat{a}_0^\dagger\hat{a}_0 + u_0u_1\hat{a}_0^\dagger\hat{a}_1 + u_1u_0\hat{a}_1^\dagger\hat{a}_0 + u_1u_1\hat{a}_1^\dagger\hat{a}_1)dxdy\rangle \tag{2.79}$$

$$+ \langle \int_{-\infty}^{\infty}\int_{0}^{\infty} (u_0u_0\hat{a}_0^\dagger\hat{a}_0 + u_0u_1\hat{a}_0^\dagger\hat{a}_1 + u_1u_0\hat{a}_1^\dagger\hat{a}_0 + u_1u_1\hat{a}_1^\dagger\hat{a}_1)dxdy\rangle \tag{2.80}$$

Flipping the first integral and letting $x \to -x$ we get

$$\text{Signal} = \langle \int_{-\infty}^{\infty}\int_{0}^{\infty} (-u_0u_0\hat{a}_0^\dagger\hat{a}_0 + u_0u_1\hat{a}_0^\dagger\hat{a}_1 + u_1u_0\hat{a}_1^\dagger\hat{a}_0 - u_1u_1\hat{a}_1^\dagger\hat{a}_1)dxdy\rangle \tag{2.81}$$

$$+ \langle \int_{-\infty}^{\infty}\int_{0}^{\infty} (u_0u_0\hat{a}_0^\dagger\hat{a}_0 + u_0u_1\hat{a}_0^\dagger\hat{a}_1 + u_1u_0\hat{a}_1^\dagger\hat{a}_0 + u_1u_1\hat{a}_1^\dagger\hat{a}_1)dxdy\rangle \tag{2.82}$$

$$\text{Signal} = \langle \int_{-\infty}^{\infty}\int_{0}^{\infty} 2(u_0u_1\hat{a}_0^\dagger\hat{a}_1 + u_1u_0\hat{a}_1^\dagger\hat{a}_0)dxdy\rangle \tag{2.83}$$

The state we are acting on is $|\psi\rangle = |\alpha\rangle_0 \otimes |\frac{\theta}{\sqrt{2}w_0}\alpha\rangle_1 \otimes |0\rangle_{i>1}$. Evaluating the integrals and then the expectation value we get

$$\text{Signal} = 2\sqrt{\frac{1}{2\pi}}\,\langle \hat{a}_0^\dagger\hat{a}_1 + \hat{a}_1^\dagger\hat{a}_0\rangle \tag{2.84}$$

$$= 2\sqrt{\frac{1}{2\pi}}(\alpha^*\alpha\frac{\theta}{\sqrt{2}w_0} + \alpha^*\alpha\frac{\theta}{\sqrt{2}w_0}) \tag{2.85}$$

$$= \frac{2|\alpha|^2\theta}{\sqrt{\pi}w_0} \tag{2.86}$$

$$\text{Signal} = \frac{2N\Delta x}{\sqrt{\pi}w_0} \tag{2.87}$$

As above, the noise for displacement measurements is set by the shot noise on an undisplaced beam. So, agai, we just have the noise of a coherent state: $\sqrt{N}$. Thus, we have recovered our SNR as before

$$\text{SNR}_{\text{SD}} = \frac{2\Delta x}{\sqrt{\pi}w_0}\sqrt{N} \tag{2.88}$$

2.4 Position Sensitive Detector

A PSD is a photodetector with leads on the ends of the photodiode. To calculate the signal of the the position sensitive detector we simply return to Eq. (2.76) and set Θ to

the appropriate response function. We follow a classical argument to derive a reasonable response function.

We know that the photocurrent at a given point is proportional to the power impinging on the detector at that point. We write this as $i(x) \propto P(x)$. From the figure we see that

$$i(x) = i_L + i_R \tag{2.89}$$

Moreover, the voltage of the left and right side are the same, so we know

$$i_L R_L = i_R R_R \tag{2.90}$$

We next impose a coordinate system such that our detector is centered on zero and has length $2L$. We take the total resistance of the detector material to be R. This fixes the form of our resistances as

$$R_L = R(\frac{x}{2L} + \frac{1}{2}) \tag{2.91}$$

$$R_R = R(\frac{1}{2} - \frac{x}{2L}) \tag{2.92}$$

From our established relations, we need to determine the photocurrents produced, i_L and i_R. Note that these would technically be photocurrent per unit length (or area when beam deflections are not restricted to 1D). Mathematically, we have two equations (Eq. (2.89) and Eq. (2.90)) and two unknowns(i_L and i_R), so we can solve the system. The result is

$$i_L = i(x)\left(\frac{R_R}{R_R + R_L}\right) \tag{2.93}$$

$$i_R = i(x)\left(\frac{R_L}{R_R + R_L}\right) \tag{2.94}$$

$$\tag{2.95}$$

The signal is proportional to the difference between the right and left photocurrents. Using Eq. (2.92) and Eq. (2.91) we find

$$\begin{aligned} \text{Signal} &\propto i_R - i_L \\ &\propto i(x)\left(\frac{R_L}{R_R + R_L}\right) - i(x)\left(\frac{R_R}{R_R + R_L}\right) \\ \text{Signal} &\propto i(x)\frac{x}{L} \end{aligned} \tag{2.96}$$

The takeaway is that our signal should be the photocurrent produced at some x-coordinate multiplied by x/L. So, instead of a step function response like the split detector, the PSD has a linear response function, $\Theta = x/L$ where $2L$ is the length of your PSD along the axis of beam displacement. We can easily construct a quantum mechanical version of the signal given in Eq. (2.96) as

$$\text{Signal} = \langle \int_{-\infty}^{\infty}\int_{-\infty}^{\infty} \frac{x}{L}\psi^{(-)}\psi^{(+)}dxdy\rangle \tag{2.97}$$

where our optical field is decomposed as $\psi^{(+)} = u_0\hat{a}_0 + u_1\hat{a}_1 + \sum_i u_i\hat{a}_i$. Where all the modes with $i > 1$ are in vacuum therefor $\langle \hat{a}_i^\dagger \hat{a}_i\rangle = 0$. So, we have

$$\text{Signal} = \langle \int_{-\infty}^{\infty}\int_{-\infty}^{\infty} \frac{x}{L}(u_0u_0\hat{a}_0\hat{a}_0 + u_0u_1\hat{a}_0\hat{a}_1 + u_1u_0\hat{a}_1\hat{a}_0 + u_1u_1\hat{a}_1\hat{a}_1)dxdy\rangle \tag{2.98}$$

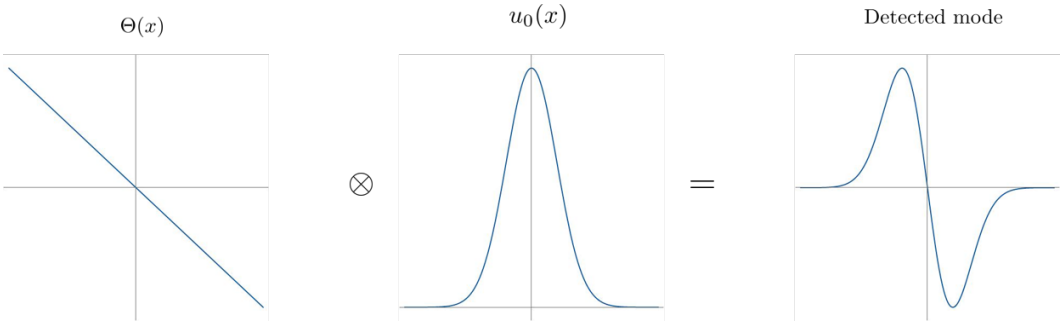

Figure 2.6: Detector mode multiplied by the transverse optical mode yields the detected mode.

Next, we use the fact that any odd function integrated over the whole domain will be zero. Thus, we are left with

$$\text{Signal} = \langle \int_{-\infty}^{\infty} \int_{-\infty}^{\infty} \frac{x}{L} (u_0 u_1 \hat{a}_0 \hat{a}_1 + u_1 u_0 \hat{a}_1 \hat{a}_0) dx dy \rangle \tag{2.99}$$

Then, using the definition of the modes given above, we have

$$\begin{aligned} \text{Signal} &= \frac{\sqrt{2} w_0}{2L} \langle \hat{a}_0^\dagger \hat{a}_1 + \hat{a}_1^\dagger \hat{a}_0 \rangle && (2.100) \\ &= \frac{\sqrt{2} w_0}{2L} (\alpha^* \alpha \frac{\theta}{\sqrt{2} w_0} + \alpha \alpha^* \frac{\theta}{\sqrt{2} w_0}) && (2.101) \\ &= \frac{|\alpha|^2 \theta}{L} && (2.102) \\ &= \frac{N \Delta x}{L} && (2.103) \end{aligned}$$

again using the fact that $|\alpha|^2 = N$. Now, to calculate the noise, we return to Eq. (2.97). By calculating the variance of this operator for an undisplaced coherent state and then taking the square root of that expression we will arrive at our noise level.

$$\begin{aligned} \text{Noise} &= \sqrt{\langle (\frac{\sqrt{2} w_0}{2L} (\hat{a}_0^\dagger \hat{a}_1 + \hat{a}_1^\dagger \hat{a}_0))^2 \rangle} && (2.104) \\ &= \frac{w_0 \sqrt{N}}{\sqrt{2} L} && (2.105) \\ & && (2.106) \end{aligned}$$

Thus, the SNR is given as

$$\text{SNR}_{\text{PSD}} = \frac{\sqrt{2} \sqrt{N} \Delta x}{w_0} \tag{2.107}$$

Comparing this expression to Eq. (2.88) we will arrive at our main result.

$$\frac{\text{SNR}_{\text{PSD}}}{\text{SNR}_{\text{SD}}} = \frac{\frac{\sqrt{2}\sqrt{N}\Delta x}{w_0}}{\frac{2\sqrt{N}\Delta x}{\sqrt{\pi} w_0}} = \sqrt{\frac{\pi}{2}} \tag{2.108}$$

Experimentally, the SNR will be measured in the deciBel scale. Thus, we should be able to observe an improvement of $10\log_{10}\sqrt{\frac{\pi}{2}} \approx 1.96$dB in the SNR of the PSD as compared to the SD. Our final result is interesting because it tells us that the position sensitive detector is slightly better than a split detector at detecting small beam displacements and should thus be the preferential detector for experimentalists attempting to work at, or below, the SQL. A flaw in our analysis, however, was in treating the currents within the detectors as classical values. Given more time on the project, we would have done a fully quantum analysis. Thus, the reader is encouraged to accept the above formalism for its generally applicability to various detector set-ups while noting that the electric current should be quantized and treated quantum mechanically.

2.5 Conclusion

In this project, we have added some theoretical detail to the derivations sketched by Barnett et. al. [27] and extended their analysis to the case of position sensitive detectors. We introduced a very general method of deriving the displacement of a coherent state by any passive optical element. This formalism will be useful to those attempting to derive the theoretical limits of their beam displacement measurements – a task of great interest to the quantum measurement community. Finally we have shown theoretically that the PSD should outperform the SD by roughly 2 dB, a result expected when one examines the Quantum Cramer-Rao Bound for the measurement. [28, 29, 31–33] This concludes the technical aspect of this thesis. We now turn to a brief overview of the academic activities I took part in outside of University of Birmingham.

Chapter 3

Conferences

3.1 Quantum Information and Measurement V: Quantum Technologies

In order to network and to learn more about the cutting edge of quantum information and measurement, I decided to attend the Optical Society if America's Quantum Information and Measurement conference in Rome, Italy. Of the many fantastic talks at the conference, a few stood out as truly exceptional in either quality or relevance to this thesis, or both. A plenary talk entitled "Gravitational-wave Detectors" was given by Nergis Mavalvala of MIT. It was a fantastic overview of the quantum optics and measurement techniques needed to detect gravitational waves. It was obviously very applicable to my research; however a thesis talk entitled "Frequency-dependent squeezed states for gravitational-wave detection through EPR entanglement" by Jan Gniesmer was even more applicable. In fact, his PhD was an experimental demonstration of the theory that forms the bulk of this thesis.

In addition to these great gravitational-wave-related talks, I also learned a great deal about quantum computing, a field that has interested me for some time. Specifically, there were several talks regarding optical quantum computing using multi-partite entanglement that really excited me. Because I love quantum optics and quantum computing, I was excited to learn that many groups around the world are attempting to develop large-scale optical quantum computers. This seems like it could be an ideal field for me to try and get some experience in throughout my PhD as it blends all of my current interests.

Overall, the conference was beneficial to my career development because I developed a picture of what fields are actively being pursued by the best researchers in the world. This is especially important to me because I am returning to the United States for my PhD. In the US, thesis projects are not decided until roughly the second year of the PhD. As such, this conference was useful because it gave me ideas for potential thesis projects, which in turn will help me with the all-important task of selecting a thesis advisor. In short, it was a wonderful opportunity to learn physics and to help guide my graduate career. Oh, and Rome wasn't so bad either.

Figure 3.1: The 2018-2019 MRes Translational Quantum Technology cohort outside the physics building at La Sapienza University of Rome.

3.2 Les Houches Predoctoral School

I was very fortunately selected for a week-long school on *Light Matter Interaction in Dilute Media and Individual Quantum Systems* organized by Quentin Glorieux (Laboratoire Kastler Brossel – Sorbonne Université), Antoine Browaeys (Institut d'Optique – Saclay University), and Julien Laurat (Laboratoire Kastler Brossel – Sorbonne Université). This turned out to be one of the most beneficial and enjoyable experiences of my time in the UK.

Each day, we had five hours of lectures and a four hour break to hike in the mountains nearby. After dinner on Monday and Wednesday we had the poster sessions. Throughout the week, I made several friends and learned a great deal about how European physics differs from the United States. Equally importantly, there was a fantastic series of lectures on "Multimode Quantum Optics" given by Nicolas Treps. His lectures were wonderfully rigorous and mathematical and will surely help with both of my projects in this thesis. Moreover, it inspired me to do quantum optics with the same rigor that seems completely standard in France. After speaking with Nicolas and Quentin, it seems I may be able to go work with Nicolas on his quantum information and measurement efforts. I hope to do so via the National Science Foundation's GRaduate Opportunities Worldwide (GROW) program.

That week in the alps made me feel like a real scientist, a feeling that not all graduate opportunities instill within their participants. It left me feeling motivated and refreshed as well as excited for the future. I hope that it will lead to real collaboration and friendship as it seems it will. Time will tell. Regardless, I can't think of a better way to spend a week.

Figure 3.2: The main building at L'École de Physique des Houches. The school was founded in 1951 by a young French scientist named Cécile DeWitt-Morette.

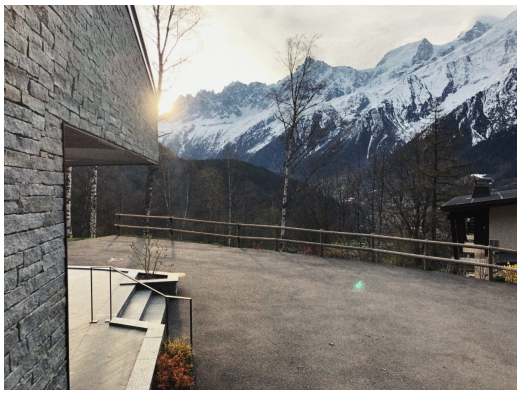

Figure 3.3: The stunning view of the mountains on my walk to breakfast.

Figure 3.4: A wonderful lecture by Robert Löw on four-wave mixing in Rubidium-87 vapor.

Bibliography

[1] Jacob L. Beckey, Yiqiu Ma, Vincent Boyer, and Haixing Miao. Broadband quantum noise reduction in future long baseline gravitational-wave detectors via epr entanglement. *Phys. Rev. D*, 100:083011, Oct 2019.

[2] B.P. Abbott et. al. Observation of Gravitational Waves from a Binary Black Hole Merger. *Phys. Rev. Lett.*, 116:061102, Feb 2016.

[3] B.P. Abbott et. al. GW151226: Observation of Gravitational Waves from a 22-Solar-Mass Binary Black Hole Coalescence. *Phys. Rev. Lett.*, 116:241103, Jun 2016.

[4] B.P. Abbott et. al. GW170814: A Three-Detector Observation of Gravitational Waves from a Binary Black Hole Coalescence. *Phys. Rev. Lett.*, 119:141101, Oct 2017.

[5] Michele Punturo. ET Conceptual Design Document.

[6] Cosmic explorer, 2019.

[7] B. P. Abbott et. al. Exploring the sensitivity of next generation gravitational wave detectors. *Classical and Quantum Gravity*, 34(4):044001, jan 2017.

[8] David Mason, Junxin Chen, Massimiliano Rossi, Yeghishe Tsaturyan, and Albert Schliesser. Continuous force and displacement measurement below the standard quantum limit. *Nature Physics*, 15(8):745–749, 2019.

[9] H. J. Kimble et. al. Conversion of conventional gravitational-wave interferometers into quantum nondemolition interferometers by modifying their input and/or output optics. *Phys. Rev. D*, 65:022002, Dec 2001.

[10] Yiqiu Ma, Haixing Miao, Belinda Heyun Pang, Matthew Evans, Chunnong Zhao, Jan Harms, Roman Schnabel, and Yanbei Chen. Proposal for gravitational-wave detection beyond the standard quantum limit through epr entanglement. *Nature Physics*, 13(8):776–780, 2017.

[11] Christopher C. Gerry and Peter L. Knight. *Introductory quantum optics*. Cambridge Univ. Press, 2008.

[12] Rodney Loudon. *The quantum theory of light*. Oxford University Press, 2004.

[13] H.A. Bachor and T.C. Ralph. *A Guide to Experiments in Quantum Optics, 2nd, Revised and Enlarged Edition*. Wiley-VCH, 2004.

[14] P. A. M. Dirac. The quantum theory of the emission and absorption of radiation. *Proceedings of the Royal Society A: Mathematical, Physical and Engineering Sciences*, 114(767):243–265, 1927.

[15] Robert Bennett, Thomas M Barlow, and Almut Beige. A physically motivated quantization of the electromagnetic field. *European Journal of Physics*, 37(1):014001, oct 2015.

[16] Claude Fabre and Nicolas Treps. Modes and states in quantum optics, 2019.

[17] Reid. Demonstration of the Einstein-Podolsky-Rosen paradox using nondegenerate parametric amplification. *Physical review. A, General physics*, 40(2):913–923, 1989.

[18] Jan Südbeck, Sebastian Steinlechner, Mikhail Korobko, and Roman Schnabel. Demonstration of interferometer enhancement through einstein–podolsky–rosen entanglement, Feb 2020.

[19] Kip S. Thorne and Roger D. Blandford. *Modern classical physics: optics, fluids, plasmas, elasticity, relativity, and statistical physics*. Princeton University Press, 2017.

[20] Carlton M. Caves and Bonny L. Schumaker. New formalism for two-photon quantum optics. i. quadrature phases and squeezed states. *Physical Review A*, 31(5):3068–3092, 1985.

[21] A. Einstein, B. Podolsky, and N. Rosen. Can Quantum-Mechanical Description of Physical Reality Be Considered Complete? *Phys. Rev.*, 47:777–780, May 1935.

[22] Brian E. Anderson et. al. Optimal phase measurements with bright- and vacuum-seeded SU(1,1) interferometers. *Phys. Rev. A*, 95:063843, Jun 2017.

[23] Denis Martynov, Haixing Miao, Huan Yang, Francisco Hernandez Vivanco, Eric Thrane, Rory Smith, Paul Lasky, William E East, Rana Adhikari, Andreas Bauswein, et al. Exploring the sensitivity of gravitational wave detectors to neutron star physics. *arXiv preprint arXiv:1901.03885*, 2019.

[24] Alessandra Buonanno and Yanbei Chen. Scaling law in signal recycled laser-interferometer gravitational-wave detectors. *Phys. Rev. D*, 67:062002, Mar 2003.

[25] Daniel D. Brown et. al. Broadband sensitivity enhancement of detuned dual-recycled Michelson interferometers with EPR entanglement. *Phys. Rev. D*, 96:062003, Sep 2017.

[26] F. Ya. Khalili. Quantum variational measurement in the next generation gravitational-wave detectors. *Phys. Rev. D*, 76:102002, Nov 2007.

[27] S.m. Barnett, C. Fabre, and A. Maıtre. Ultimate quantum limits for resolution of beam displacements. *The European Physical Journal D*, 22(3):513–519, 2003.

[28] N. Treps, U. Andersen, B. Buchler, P. K. Lam, A. Maître, H.-A. Bachor, and C. Fabre. Surpassing the standard quantum limit for optical imaging using nonclassical multimode light. *Physical Review Letters*, 88(20), 2002.

[29] Olivier Pinel, Julien Fade, Daniel Braun, Pu Jian, Nicolas Treps, and Claude Fabre. Ultimate sensitivity of precision measurements with intense gaussian quantum light: A multimodal approach. *Physical Review A*, 85(1), 2012.

[30] Roy J. Glauber. The quantum theory of optical coherence. *Phys. Rev.*, 130:2529–2539, Jun 1963.

[31] Hengxin Sun, Kui Liu, Zunlong Liu, Pengliang Guo, Junxiang Zhang, and Jiangrui Gao. Small-displacement measurements using high-order hermite-gauss modes. *Applied Physics Letters*, 104(12):121908, 2014.

[32] Magnus T L Hsu, Vincent Delaubert, Ping Koy Lam, and Warwick P Bowen. Optimal optical measurement of small displacements. *Journal of Optics B: Quantum and Semiclassical Optics*, 6(12):495–501, oct 2004.

[33] C.w. Helstrom. Minimum mean-squared error of estimates in quantum statistics. *Physics Letters A*, 25(2):101–102, 1967.

Appendix A

Quantum Optics Derivations

A.1 Derivation of NLA Input-Output Relation

The interaction Hamiltonian of nondegenerate parametric amplifier is given as

$$\hat{H}_{int} = i\hbar\chi^{(2)}\alpha_p\big(a^\dagger b^\dagger - ab\big) \tag{A.1}$$

where $\chi^{(2)}$ is the nonlinear susceptibility of the medium, α_p is the pump amplitude, and a and b are the signal and idler modes, respectively. We now solve the Heisenberg equations of motion for the signal and idler.

$$\begin{aligned}
\dot{a} &= \frac{1}{i\hbar}[a, H_{int}] \\
&= \chi^{(2)}\alpha_p\Big(a\big(a^\dagger b^\dagger - ab\big) - \big(a^\dagger b^\dagger - ab\big)a\Big) \\
&= \kappa\Big(aa^\dagger b^\dagger - aab - a^\dagger b^\dagger a + aba\Big) \\
&= \kappa\Big((aa^\dagger - a^\dagger a)b^\dagger\Big) \\
&= \kappa[a, a^\dagger]b^\dagger \\
\dot{a} &= \kappa b^\dagger
\end{aligned}$$

Following the exact same steps gives $\dot{b} = \kappa a^\dagger$. The second derivatives are then

$$\ddot{a} = \kappa\dot{b}^\dagger \tag{A.2}$$

$$\ddot{a} = \kappa^2 a \tag{A.3}$$

and

$$\ddot{b} = \kappa^2 b \tag{A.4}$$

Let's solve eq. 1.3 first. Assume a solution $a(t) = e^{\lambda t}$. This leads to the characteristic equation $\lambda^2 - \kappa^2 = 0$ or $\lambda = \pm\kappa$. So our solution is simply

$$a(t) = A'e^{-\kappa t} + B'e^{\kappa t} \tag{A.5}$$

Now, typically we would apply boundary conditions and be done; however, it is common in the field of quantum optics to instead parameterize the above function as

$$a(t) = A\sinh\kappa t + B\cosh\kappa t \tag{A.6}$$

which we can get by just letting $A' = \frac{B-A}{2}$ and $B' = \frac{A+B}{2}$. This is allowed because these constants are still just constants and will therefore be solutions to the differential equation. We need the derivative of (1.6) as well.

$$\dot{a}(t) = A\kappa\cosh\kappa t - B\kappa\sinh\kappa t \tag{A.7}$$

and

$$\dot{a}(t) = \kappa b^\dagger \tag{A.8}$$

Now we apply the boundary conditions $a(0) = B$ and $\dot{a}(0) = A\kappa = \kappa b^\dagger(0) \implies A = b^\dagger(0)$. So we have

$$a(t) = a(0)\cosh\kappa t + b^\dagger(0)\sinh\kappa t \tag{A.9}$$

We can follow the exact same procedure to find

$$b(t) = b(0)\cosh\kappa t + a^\dagger(0)\sinh\kappa t \tag{A.10}$$

Following the two photon formalism of Carlton Caves, we define the amplitude and phase quadratures as

$$a_1(t) = \frac{a(t) + a^\dagger(t)}{\sqrt{2}} \tag{A.11}$$

$$a_2(t) = \frac{a(t) - a^\dagger(t)}{\sqrt{2}i} \tag{A.12}$$

Plugging (1.9) and (1.10) into these definitions, we get

$$a_1(t) = \frac{1}{\sqrt{2}}\big(a(0)\cosh\kappa t + b^\dagger(0)\sinh\kappa t + a^\dagger(0)\cosh\kappa t + b(0)\sinh\kappa t\big) \tag{A.13}$$

$$a_1(t) = a_1(0)\cosh\kappa t + b_1(0)\sinh(\kappa t) \tag{A.14}$$

$$\tag{A.15}$$

$$b_1(t) = b_1(0)\cosh\kappa t + a_1(0)\sinh(\kappa t) \tag{A.16}$$

Now, let's look at the so-called amplitude difference quadrature $X_-(t) = a_1(t) - b_1(t)$

$$X_-(t) = a_1(t) - b_1(t) \tag{A.17}$$

$$= a_1(0)\cosh\kappa t + b_1(0)\sinh(\kappa t) - (b_1(0)\cosh\kappa t + a_1(0)\sinh(\kappa t)) \tag{A.18}$$

$$= e^{-\kappa t}a_1(0) - e^{-\kappa t}b_1(0) \tag{A.19}$$

$$= e^{-\kappa t}X_-(0) \tag{A.20}$$

It follows that the uncertainty associated with this state is less after the amplifier:

$$\langle\Delta^2 X_-(t)\rangle = \langle X_-(t)^2\rangle - \langle X_-(t)\rangle^2 \tag{A.21}$$

$$= \langle(e^{-\kappa t}X_-(0))^2\rangle - \langle e^{-\kappa t}X_-(0)\rangle^2 \tag{A.22}$$

$$= e^{-2\kappa t}(\langle X_-(0)^2\rangle - \langle X_-(0)\rangle^2) \tag{A.23}$$

$$\Delta X_-(t) = e^{-\kappa t}\Delta X_-(0) \tag{A.24}$$

We have the exact same relationship for the phase sum quadrature:

$$\Delta P_+(t) = e^{-\kappa t}\Delta P_+(0) \tag{A.25}$$

A.2 Spectral Density Calculation Example

Here we will calculate one element from the spectral density matrix given in section 1.2.5. From our definition of spectral density (eq. 1.13) we have

$$\begin{aligned}
S_{\hat{a}_1\hat{a}_1}\delta(\Omega-\Omega') &= \frac{1}{2\pi}\langle\xi|\,\hat{a}_1\hat{a}_1^\dagger + \hat{a}_1^\dagger\hat{a}_1\,|\xi\rangle \\
&= \frac{1}{2\pi}\langle 0|\,\hat{S}^\dagger(\hat{a}_1\hat{a}_1^\dagger + \hat{a}_1^\dagger\hat{a}_1)\hat{S}\,|0\rangle \\
&= \frac{1}{2\pi}\langle 0|\,\hat{S}^\dagger\hat{a}_1\hat{S}\hat{S}^\dagger\hat{a}_1^\dagger\hat{S} + \hat{S}^\dagger\hat{a}_1^\dagger\hat{S}\hat{S}^\dagger\hat{a}_1\hat{S}\,|0\rangle \\
&= \frac{1}{2\pi}\langle 0|\,\hat{S}^\dagger(\frac{\hat{a}_+ + \hat{a}_-^\dagger}{\sqrt{2}})\hat{S}\hat{S}^\dagger(\frac{\hat{a}_+^\dagger + \hat{a}^-}{\sqrt{2}})\hat{S} + \hat{S}^\dagger(\frac{\hat{a}_+^\dagger + \hat{a}^-}{\sqrt{2}})\hat{S}\hat{S}^\dagger(\frac{\hat{a}_+ + \hat{a}_-^\dagger}{\sqrt{2}})\hat{S}\,|0\rangle \\
&= \frac{1}{4\pi}\langle 0|\,\hat{S}^\dagger(\hat{a}_+ + \hat{a}_-^\dagger)\hat{S}\hat{S}^\dagger(\hat{a}_+^\dagger + \hat{a}_-)\hat{S} + \hat{S}^\dagger(\hat{a}_+^\dagger + \hat{a}_-)\hat{S}\hat{S}^\dagger(\hat{a}_+ + \hat{a}_-^\dagger)\hat{S}\,|0\rangle
\end{aligned}$$

Expanding this out will give us terms like $\hat{S}^\dagger\hat{a}_+\hat{S}$ which we know how to transform using equations 1.11 and 1.12. Applying these and using the fact that $\hat{a}_\pm\,|0\rangle = 0$ we get

$$\begin{aligned}
S_{\hat{a}_1\hat{a}_1}\delta(\Omega-\Omega') &= \frac{1}{4\pi}\langle 0|\,\hat{a}_+\hat{a}_+^\dagger\cosh^2 r + \hat{b}_+\hat{b}_+^\dagger\sinh^2 r\,|0\rangle \\
&= \frac{1}{4\pi}(2\pi\delta(\Omega-\Omega')(\cosh^2 r + \sinh^2 r)) \\
S_{\hat{a}_1\hat{a}_1} &= \frac{1}{2}(\cosh^2 r + \sinh^2 r) \\
&= \frac{1}{2}\cosh 2r
\end{aligned}$$